

# *J*-driven Dynamic Nuclear Polarization for sensitizing high field solution state NMR

*Maria Grazia Concilio*<sup>1\*</sup>, *Ilya Kuprov*<sup>2</sup>, *Lucio Frydman*,<sup>1,3\*</sup>

<sup>1</sup>Department of Chemical and Biological Physics, Weizmann Institute of Science, Rehovot, Israel.

<sup>2</sup>School of Chemistry, University of Southampton, Southampton, UK.

<sup>3</sup>National High Magnetic Field Laboratory, Tallahassee, Florida, USA.

## **Abstract**

Dynamic nuclear polarization (DNP) is widely used to enhance solid state nuclear magnetic resonance (NMR) sensitivity. Its efficiency as a generic signal-enhancing approach for liquid state NMR, however, decays rapidly with magnetic field  $B_0$ , unless mediated by scalar interactions arising only in exceptional cases. This has prevented a more widespread use of DNP in structural and dynamical solution NMR analyses. This study introduces a potential solution to this problem, relying on biradicals with exchange couplings  $J_{\text{ex}}$  of the order of the electron Larmor frequency  $\omega_E$ . Numerical and analytical calculations show that in such  $J_{\text{ex}} \approx \pm \omega_E$  cases a phenomenon akin to that occurring in chemically induced DNP (CIDNP) happens, leading to different relaxation rates for the biradical singlet and triplet states hyperfine-coupled to the nuclear  $\alpha$  or  $\beta$  states. Microwave irradiation can then generate a transient nuclear polarization build-up with high efficiency, at all magnetic fields that are relevant in contemporary NMR, and for all rotational diffusion correlation times that occur in small- and medium-sized molecules in conventional solvents.

Corresponding authors:

\*[maria-grazia.concilio@weizmann.ac.il](mailto:maria-grazia.concilio@weizmann.ac.il)

\*[lucio.frydman@weizmann.ac.il](mailto:lucio.frydman@weizmann.ac.il)

## 1. Introduction

Higher NMR sensitivity could bring transformative breakthroughs to analytical, pharmaceutical and biophysical chemistry. NMR sensitivity can be enhanced by higher external magnetic fields  $B_0$ , but this is a slow, expensive approach. An alternative arises if electron magnetization is transferred, from a stable radical, to the nuclei to be detected. By irradiating electrons near their Larmor frequency,  $\omega_E$ , the so-called Dynamic Nuclear Polarization (DNP) effect can then enhance NMR sensitivity up to the  $\gamma_E/\gamma_N$  gyromagnetic ratio, typically by factors of 100- to 1000-fold. Predicted by Overhauser in 1953<sup>1</sup> and thereafter confirmed by Carver and Slichter,<sup>2</sup> DNP has revolutionized solid state NMR;<sup>3-6</sup> it has also made inroads into *in vivo* spectroscopy, based on rapid melting approaches.<sup>7,8</sup> DNP, however, has not yet impacted what is arguably the widest of NMR realms – high-field solution-state studies. This longstanding problem arises from Overhauser DNP efficiency that in liquids depends on the electron-nuclear cross-relaxation rate  $\sigma_{E,N}$ :

$$\sigma_{E,N} \approx \frac{\gamma_E^2 \gamma_N^2 \hbar^2}{10} \left( \frac{\mu_0}{4\pi} \right)^2 \frac{\tau_C}{r_{EN}^6} \left( \frac{6}{1 + (\omega_E + \omega_N)^2 \tau_C^2} - \frac{1}{1 + (\omega_E - \omega_N)^2 \tau_C^2} \right) \quad (1)$$

which decreases quadratically with the  $B_0$ . In non-viscous liquids the rotational correlation time of a typical molecule is  $\tau_C \approx 0.1$ -1 ns, while electron Larmor frequencies are  $\omega_E \approx 300$  GHz, leading to  $(\omega_E \pm \omega_N)^2 \tau_C^2 \gg 1$  and negligible cross-relaxation rates in Eq. (1). Consequently – and unless aided by the contact couplings that can arise for certain radicals and solutes<sup>9-13</sup> – typical <sup>1</sup>H DNP enhancements drop to a maximum of  $\approx 330x$  when  $B_0 \leq 0.4T$ , to  $\approx 1.001x$  at the  $\geq 7$  T fields where contemporary NMR is done.<sup>9,14-17</sup> We recently discussed a way to bypass these spectral power density bottlenecks based on a cross-correlated (CC) DNP strategy involving biradicals as polarization sources.<sup>18</sup> CCDNP, however, required significant coincidences between nuclear/electron spin interaction tensors, and long-term stability in the nuclear-electron geometry; for optimal conditions, it then provided steady-state NMR enhancements that approached  $\approx 10$ -20x.

This study reports a further investigation into the physics of a three-spin biradical/nuclear system, revealing a new polarization transfer possibility. Unlike CCDNP, the mechanism that is here introduced: (i) does not put stringent conditions on multiple independent coupling tensors; (ii) can lead to nuclear polarization enhancements of  $\approx 100$ -200x for  $B_0$  ranging from  $\leq 1T$  to  $\geq 20$  T and for rotational correlation times in the 0.1 - 1 ns range; and (iii) does not result from a steady state upon electron saturation, but rather from transient phenomena. At the centre of this proposal are two electrons interacting through an exchange coupling  $J_{ex}$  of the order of  $\omega_E$ , a chemically tuneable condition that can be fulfilled by many biradicals known to have exchange couplings in the  $0 \leq J_{ex} \leq 1$  THz range.<sup>19-21</sup> Under such conditions we found that moderate microwave ( $\mu W$ ) fields can lead to the DNP enhancement improvements shown in Figure 1. The present study demonstrates and explains the basis of this J-driven (J-DNP) mechanism based on Liouville space numerical simulations and analytical calculations using Redfield's relaxation theory<sup>22-26</sup>. The latter serve to highlight similarities between the roles that the electronic singlet and triplet states play in polarizing nuclei in J-DNP, and those played by singlet and triplet states arising in chemically-induced DNP (CIDNP) experiments.<sup>27-30</sup>

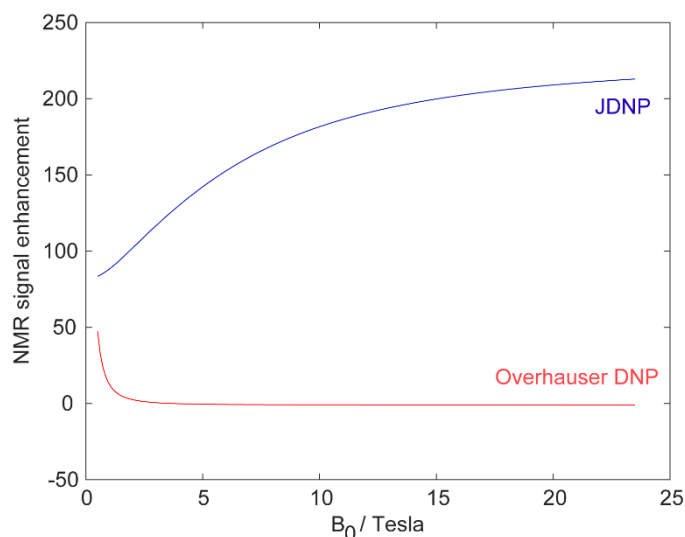


**Fig. 1:** Comparison between the maximal enhancements delivered by the Overhauser and by J-driven DNP, as function of  $B_0$ . The J-DNP simulation was performed using a biradical/proton triad with a  $\tau_c = 500$  ps rotational correlation time, a  $J_{ex} = +(\omega_E + \omega_N)$  at each field strength, and other parameters as given in Table 1. The Overhauser DNP simulation was performed for a two-spin electron/proton dipole-coupled pair with  $\tau_c = 157$  ps (typical of trityl<sup>31</sup>) and other parameter as given in Table 1, but with one of the electrons in the Table absent.

## 2. Features of J-DNP

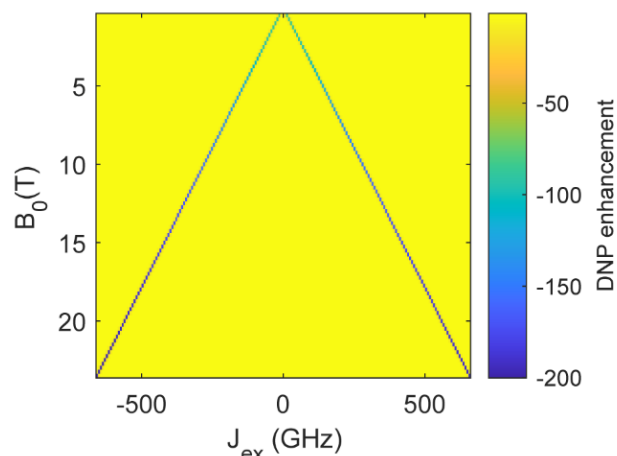
The system examined in this work corresponds to a biradical interacting with a proton exclusively through dipolar (*aka* anisotropic hyperfine) couplings. The spin system has two unpaired spin-1/2 electrons belonging to the same molecule, and a spin-1/2 proton placed 8.6 Å away from the first electron and 11.1 Å away from the second electron (see Table 1 for the actual proton and electron coordinates). The two electrons are assumed to have identical  $g$ -tensors (assumed anisotropic for the sake of realism, even if the Supporting Information shows that neither nuclear shielding anisotropy nor  $g$ -anisotropy are required for the J-DNP enhancement). All dipolar couplings were computed from Cartesian coordinates. Scalar electron-nuclear couplings were set to zero. The most important variable in the system is the isotropic inter-electron exchange coupling  $J_{ex}$ , which was modelled on the basis of trityl-based symmetric biradicals for which such couplings have been observed.<sup>19,20</sup> These parameters were used to create the spin Hamiltonian, and to calculate the evolution subject to microwave irradiation and relaxation as per Redfield's theory.<sup>22,25</sup> (See Supporting Information 1 for additional discussion of these radicals, including their estimated solution-state  $T_{1s}$  and  $T_{2s}$ .<sup>32,33</sup>)

**Table 1:** Biradical / proton parameters used in the simulations shown in Figures 1 - 5.  $B_0$ ,  $J_{ex}$  and  $\tau_c$  were set as described in the figures; all other coupling parameters relied on the inter-spin distances.

Parameter	Value
<sup>1</sup> H chemical shift tensor, ppm	[5 10 20]
$g$ -tensor <sup>1</sup> for electrons 1 and 2, Bohr magneton	[2.0032 2.0032 2.0026]
<sup>1</sup> H coordinates, [x y z], Å	[-3 0.5 1.3]
Electron 1 coordinates, [x y z], Å	[0 0 -9.37]
Electron 2 coordinates, [x y z], Å	[0 0 9.37]
Scalar relaxation modulation depth, GHz	3
Scalar relaxation modulation time, ps	1
Microwave nutation frequency, $\omega_{\mu W}$ , MHz	1
Temperature, K	298

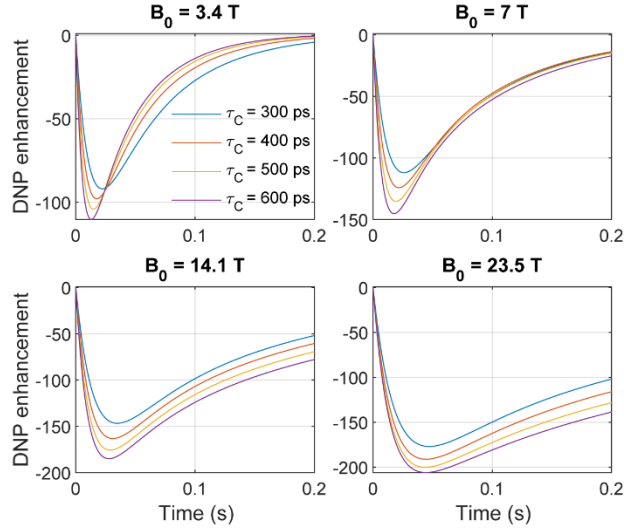
<sup>1</sup> Simulations used identical Zeeman interaction tensors, that were made axially symmetric along the main molecular axis (corresponding the linker connecting the two trityls).

Figure 2 shows how the isotropic exchange coupling modulates the maximum nuclear enhancement achievable by J-DNP, as a function of magnetic field  $B_0$ . These numerically simulated plots<sup>34</sup> predict that, for every field strength, there are two  $J_{\text{ex}} = \pm(\omega_E + \omega_N)$  values for which microwave irradiation leads to a nuclear enhancement close to the maximum  $\gamma_E/2\gamma_N$  value achievable.



**Fig. 2:** Simulated DNP enhancement achieved within 20 ms of microwave irradiation as a function of  $J_{\text{ex}}$  and  $B_0$ . The plots arise from time domain simulations using the parameters in Table 1, a biradical/proton triad  $\tau_c = 500$  ps, and an on-resonance irradiation at the electron Larmor frequency of the biradicals. In this and other graphs shown below, DNP enhancements denote the achieved nuclear polarization, normalized by its Boltzmann counterpart at the same temperature and field.

Unlike Overhauser DNP and CCDNP enhancements,<sup>18</sup> nuclear polarization enhancements shown in Figure 2 and arising at the  $J_{\text{ex}} = \pm(\omega_E + \omega_N)$  conditions, are transient phenomena. This is illustrated in Figure 3, which shows the enhancement's time-dependence for different rotational correlation times and magnetic fields, for spin systems with an optimally chosen  $J_{\text{ex}} = +(\omega_E + \omega_N)$  coupling subject to continuous microwave irradiation. These graphs show a nuclear polarization that rapidly builds up and then decays into steady states which, at the usual NMR fields used in analytical/biophysical studies, are essentially Boltzmann equilibrium nuclear magnetization. In all cases, substantial transient enhancements are observed after 10-50 ms of irradiation, with precise timings and maximal values that depend on  $B_0$  and on the correlation time  $\tau_c$  of the biradical/proton triad. These behaviours are radically different from those of Overhauser DNP. Additional differences between the behaviours of Overhauser and J-DNP are discussed in Fig. S3 of Supporting Information 1, which compares expectations from a two-spin proton/electron system (Overhauser DNP), and the changes arising when a second  $J$ -coupled electron is added to form a biradical with  $J_{\text{ex}} = +(\omega_E + \omega_N)$ . Upon introducing a second electron, similarly weak steady-state nuclear polarization values are reached – but on the way to those steady states, there are strong transient enhancements. In fact, in Figure 3, these transient enhancements improve slightly with both higher  $B_0$ s and slower  $\tau_c$ s of the biradical/proton triad.



**Fig. 3:** Time domain simulations showing the evolution of the DNP enhancement observed under continuous microwave irradiation of the electrons, for an array of  $B_0$  and of  $\tau_c$  values of the biradical/proton triad. For all fields  $J_{ex}$  was set to  $+(\omega_E + \omega_N)$ ; other simulation parameters are as given in Table 1.

### 3. The Physics of J-DNP

The physics that drives the J-DNP effects, summarized in Figures 2-5, is reminiscent of the cross-correlation CIDNP mechanism. According to the radical pair theory,<sup>28,29,35</sup> nuclear magnetization enhancement in CIDNP proceeds from three processes: (i) singlet/triplet interconversion within a spin-correlated biradical; (ii) a modulation of the rate of this interconversion by hyperfine couplings (i.e. differently, depending on whether the nuclear spin state is  $\alpha$  or  $\beta$ ); and (iii) rapid nuclear spin relaxation in the unreacted triplet biradical acting as a nuclear spin state filter. In the J-DNP case, the biradical is not (photo)chemically produced and does not recombine after a transient action; still, the singlet-triplet behaviour vis-à-vis the nuclear spin once again becomes relevant. In the J-DNP case, it is microwaves (rather than a laser) that drive the system away from the thermal equilibrium. As in CIDNP, it is essential that the nucleus is differentially hyperfine-coupled to the two electrons for the J-DNP enhancement to occur (the effect disappears otherwise, see Supporting information 6). It is the different relaxation characteristics of the ensuing singlet/triplet electronic states when facing the nuclear  $\alpha$  or  $\beta$  states, that build up the nuclear polarization.

To translate these features into a representative description, the two coupled electrons were assumed to have identical  $g$ -factors. In such  $J_{ex} \gg \omega_{\Delta e}$  case, where  $\omega_{\Delta e} = \omega_{e1} - \omega_{e2}$  is the difference between the Larmor frequency of the two electrons, the electron Zeeman eigenstates  $|\alpha_1\beta_{e2}\rangle$  and  $|\beta_{e1}\alpha_{e2}\rangle$  are no longer eigenfunctions of the spin Hamiltonian. We therefore express the Hamiltonian in the singlet/triplet electron basis sets. As shown in Supporting Information 2, this leads to the following microwave rotating frame Hamiltonian:

$$\hat{H}_{rot} = \hat{H}^{S_0T_0} + \hat{H}^{T_{+1}T_{-1}} + \hat{H}_{\mu w} \quad (2)$$

where  $\hat{H}^{S_0T_0}$  the Hamiltonian acting in the  $\hat{S}_0\hat{T}_0$  sub-space,  $\hat{H}^{T_{+1}T_{-1}}$  is the Hamiltonian acting in the  $\hat{T}_{+1}\hat{T}_{-1}$  sub-space, and  $\hat{H}_{\mu w}$  is the microwave operator (each term is further defined in Supporting

Information 2). With this Hamiltonian, Liouville-space time domain simulations were performed with the following equation of motion:

$$\frac{\partial}{\partial t} \hat{\rho}(t) = -i\hat{L}\hat{\rho}(t), \quad \hat{L} = \hat{H}_{\text{rot}} + i\hat{R}, \quad O(t) = \langle \hat{O} | \hat{\rho}(t) \rangle \quad (3)$$

where  $\hat{\rho}(t)$  is the state vector of the system,  $\hat{L}$  is the Liouvillian containing the rotating frame Hamiltonian superoperator with the internal plus microwave interactions, as well as the relaxation superoperator  $\hat{R}$  accounting for the stochastic rotation of all anisotropies. The latter was computed according to the Bloch-Redfield-Wangsness relaxation theory<sup>22,36</sup> both by analytical<sup>24</sup> and numerical<sup>25,26</sup> means, including all possible longitudinal, transverse and cross-correlated pathways. Since the spin system was considered at room temperature, Di-Bari - Levitt thermalization was used.<sup>37</sup> Considering that the exchange coupling has the same order of magnitude as the electron Larmor frequency, simulations took into account scalar relaxation of the first kind,<sup>38</sup> that was incorporated into the relaxation superoperator. This did not have an effect on the DNP enhancement, since in the  $\omega_{\Delta e} \rightarrow 0$  case in question, the exchange coupling,  $\hat{E}_1 \cdot \hat{E}_2$ , commutes with the Zeeman interaction,  $\hat{E}_{1Z} + \hat{E}_{2Z}$ . Time evolution  $\hat{O}(t)$  of multiple spin state populations was calculated by taking their scalar products with the state vector  $\hat{\rho}(t)$  at each time.

Figures 4a-4d show the simulated time dependencies of the three-spin population operators  $\hat{O}_{\alpha/\beta}$ , corresponding to the two-electron singlet and triplets  $\hat{T}_{\pm 1, \alpha/\beta}$ ,  $\hat{T}_{0, \alpha/\beta}$  and  $\hat{S}_{0, \alpha/\beta}$ , and a proton in either an  $\alpha$  or  $\beta$  state (see Supporting Information 3 for the expressions of these  $\hat{O}_{\alpha/\beta}$  as Cartesian operators). Figure 4e shows the states arising from the difference between  $\hat{O}_{\alpha}$  and  $\hat{O}_{\beta}$ , defined as:

$$\hat{O}^{(e1e2)} \hat{N}_Z = \left| \hat{O}^{(e1e2)} \right\rangle \left\langle \hat{O}^{(e1e2)} \right| \hat{N}_Z = \frac{1}{2} (\hat{O}_{\alpha} - \hat{O}_{\beta}) \quad (4)$$

where  $\hat{O}^{(e1e2)}$  denotes the two-electron singlet and triplet, and  $\hat{N}_Z$  is the longitudinal nuclear magnetization. Figure 4f shows the overall  $\hat{N}_Z$  amplitude calculated upon summing the amplitudes of  $\hat{S}_0 \hat{N}_Z$ ,  $\hat{T}_0 \hat{N}_Z$  and  $\hat{T}_{\pm 1} \hat{N}_Z$ , normalized to the equilibrium nuclear magnetization.

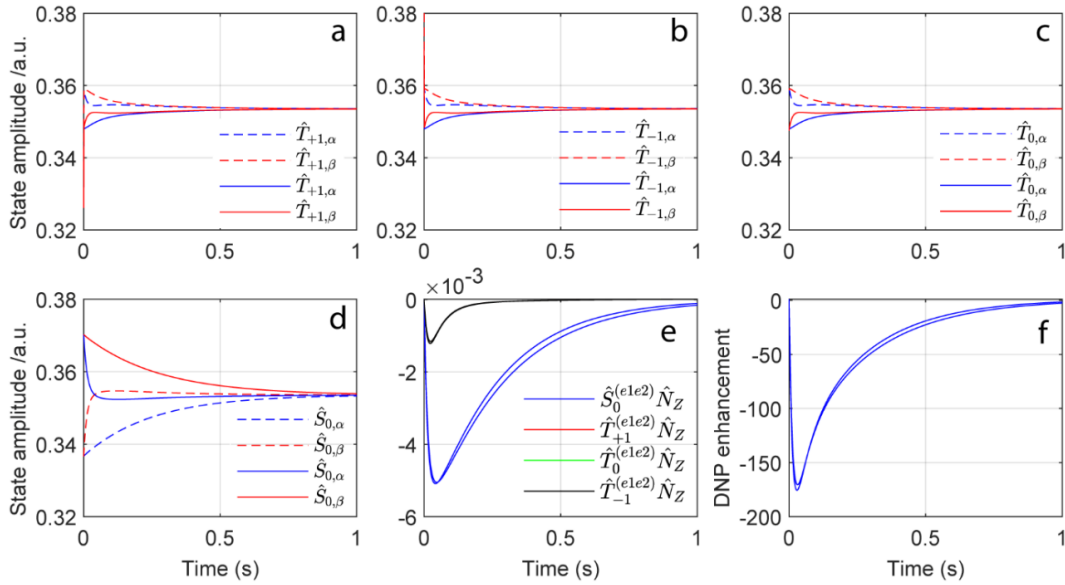


**Fig. 4:** Time evolution of the three-spin population operators:  $\hat{T}_{\pm 1, \alpha/\beta}$ ,  $\hat{T}_{0, \alpha/\beta}$  and  $\hat{S}_{0, \alpha/\beta}$  (a-d), and of the  $\hat{N}_Z \hat{S}_0$ ,  $\hat{N}_Z \hat{T}_{\pm 1}$  and  $\hat{N}_Z \hat{T}_0$  states (e) arising from the difference between the various  $\hat{O}_{\alpha}$  and  $\hat{O}_{\beta}$ . Time evolution of the overall longitudinal nuclear magnetization  $\hat{N}_Z$  (f), showing the sum of all  $\hat{N}_Z$ -related contributions, normalized by the thermal nuclear magnetization

under the same conditions. Plots (a-d) are normalized to a total electron spin population of one, as defined in Supporting Information 3.  $J_{\text{ex}} = +(\omega_{\text{E}} + \omega_{\text{N}})$  was used for the dashed lines, and  $J_{\text{ex}} = -(\omega_{\text{E}} + \omega_{\text{N}})$  was used for the continuous lines. In (e), the red and green traces are barely seen as they fall underneath an overlapping black trace. The slightly different curves in (f) reflect  $J_{\text{ex}} = \pm(\omega_{\text{E}} + \omega_{\text{N}})$  conditions, respectively. For all these calculations  $B_0 = 14.08$  T,  $\tau_c = 500$  ps for the biradical/proton triad; all other parameters as given in Table 1.

At time zero, the system is at the thermal equilibrium, and negligible differences arise between the populations of the  $\alpha$  and  $\beta$  nuclear states – even if singlet and triplet electron state populations differ. When the microwave irradiation is turned on and electron saturation sets in, the triplet states are mixed, and their populations start to converge to similar amplitudes (Figures 4a-4c). However, at the  $J_{\text{ex}} = \pm(\omega_{\text{E}} + \omega_{\text{N}})$  condition, the rates at which electron states settle into the new equilibrium is different for  $\alpha$  and  $\beta$  nuclear components: when  $J_{\text{ex}} = +(\omega_{\text{E}} + \omega_{\text{N}})$  the  $\alpha$  component of the triplets (Fig. 4, blue dashed line) reaches the steady state faster than the  $\beta$  component (red dashed line), while the  $\beta$  component of the singlet (red dashed line) reaches steady state faster than the  $\alpha$  component of the singlet (blue dashed line).<sup>39</sup> The opposite  $\alpha/\beta$  behaviour arises when  $J_{\text{ex}} = -(\omega_{\text{E}} + \omega_{\text{N}})$ . Still, because different initial conditions exist when  $J_{\text{ex}} = \pm(\omega_{\text{E}} + \omega_{\text{N}})$ , both situations lead to similar transient nuclear polarization build-ups, as shown in Figure 4e. Consequently, due to the different relaxation rates of the  $\alpha$  and  $\beta$  nuclear components of the triplet and singlet electron states, a sizable nuclear polarization  $\hat{N}_Z$  builds up. As can be appreciated in Figure 4f, this polarization is only weakly dependent on the sign of  $J_{\text{ex}}$ . Also note that, as eventually all electron/nuclear states reach the same populations, J-DNP build up is transient: no nuclear polarization gains are predicted when the steady-state conditions are examined, as is usually done in the analysis of conventional Overhauser DNP.

The plots shown in Figure 4 were computed assuming continuous microwave irradiation. To avoid the decay of the enhancement – dominated by the nuclear  $T_1$  decay draining the  $S_0Nz$  state – microwaves could be turned off when nuclear magnetization has reached a maximum; the electron population operators would then relax back to thermal equilibrium, and the build-up could be “pumped” again by repeated irradiation. However, in an actual biradical-driven enhancement experiment, the polarizing proton would not be covalently bound; rather, it would be randomly diffusing at rates of ca. 1  $\mu\text{m}/\text{ms}$ . The interaction with the polarizing biradical would thus be short-lived, and the proton would get repeatedly polarized by different transient encounters with different biradicals; a certain “pulsing” of the effect will therefore occur spontaneously.<sup>11,40,41</sup> It is also instructive to consider the maximum enhancement expected from the differences in  $R[\hat{O}_{\alpha/\beta}]$  relaxation rates. Assuming for simplicity that one of the states relaxes infinitely fast while the other has no relaxation, a simple analysis shows that, under an assumption of complete initial electron saturation, the nuclear polarization would reach a value of 0.5 – the NMR signal would be enhanced by  $|\gamma_{\text{E}}/2\gamma_{\text{N}}|$ . The data in Figures 1-4 shows  $\hat{N}_Z$  enhanced to a significant fraction of this upper bound.

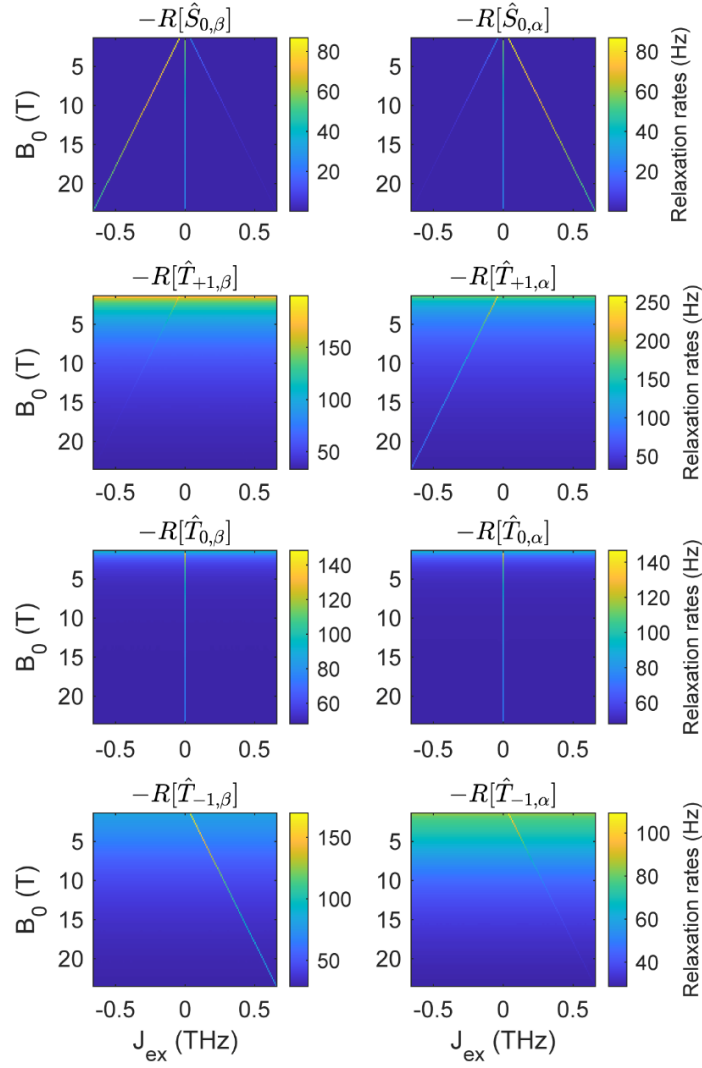


**Fig. 5:** Numerically computed (Redfield theory) self-relaxation rates of the three-spin population operators as a function of  $J_{\text{ex}}$  and  $B_0$ . Rates of  $\hat{S}_{0,\beta}$ ,  $\hat{T}_{0,\beta}$  and  $\hat{T}_{\pm 1,\beta}$  are on the left, and rates of  $\hat{S}_{0,\alpha}$ ,  $\hat{T}_{0,\alpha}$  and  $\hat{T}_{\pm 1,\alpha}$  are on the right. Calculations relied on the parameters of Table 1 and on  $\tau_c = 500$  ps for the biradical/proton triad.

Figure 5 examines another facet of J-DNP by showing how the population decay due to self-relaxation rates of the  $\hat{O}_{\alpha/\beta} = \hat{T}_{\pm 1,\alpha/\beta}$ ,  $\hat{T}_{0,\alpha/\beta}$  and  $\hat{S}_{0,\alpha/\beta}$  population operators change over a range of magnetic fields  $B_0$  and exchange couplings  $J_{\text{ex}}$ . Notice that, as expected from Overhauser DNP, electron-nuclear cross-relaxation rates are high and thus conducive to nuclear polarization enhancements only at low  $B_0$ . Although these rates become exceedingly small for  $B_0$ s of interest in NMR, marked enhancements in these rates arise whenever  $J_{\text{ex}}$  matches  $\pm(\omega_E + \omega_N)$ . Moreover, marked asymmetries also distinguish the relaxation rates of the  $\alpha$  and  $\beta$  states associated to the  $\hat{T}_{\pm 1,0}$  and  $\hat{S}_0$  states. All that is needed to highlight these enhanced, asymmetric relaxation rates is to take the electron spins out of equilibrium by microwave irradiation, and capture the nuclear enhancement before the system returns to its final,  $\alpha/\beta$ -independent, steady state saturation conditions. Supporting Information 4 provides additional information about these self-relaxation rates. Note as well that, even though the absolute values of these rates decrease with  $B_0$  and  $\tau_c$ , their differences actually remain present (Figures S4 and S5, Supporting information), and still lead to sizable longitudinal nuclear magnetizations; this helps to understand the increased efficiencies with  $B_0$  and  $\tau_c$  shown for J-DNP enhancements in Figures 1 - 4.

The trends in Figure 5 can be interpreted by considering the analytical expressions for the relaxation rates of singlet and the triplet states that can be derived from Redfield's relaxation theory.<sup>24,36</sup> As long as this theoretical model is valid ( $\tau_c \leq 2$  ns), these rates can be summarized as:

$$-R[\hat{S}_{0,\beta}] = \frac{\Delta_{\Delta\text{HF}}^2}{180} J(J_{\text{ex}} - \omega_E + \omega_N) + \frac{\Delta_{\Delta\text{HF}}^2}{30} J(J_{\text{ex}} + \omega_E + \omega_N) + \frac{[\Delta_{\Delta\text{HF}}^2 + 4\aleph_{\Delta\text{G},\Delta\text{G}-\Delta\text{HF}}]}{120} J(J_{\text{ex}} - \omega_E) + \frac{[\Delta_{\Delta\text{HF}}^2 + 4\aleph_{\Delta\text{G},\Delta\text{G}-\Delta\text{HF}}]}{120} J(J_{\text{ex}} + \omega_E) + \dots \quad (5)$$

and

$$-R[\hat{S}_{0,\alpha}] = \frac{\Delta_{\Delta\text{HF}}^2}{180} J(J_{\text{ex}} + \omega_E - \omega_N) + \frac{\Delta_{\Delta\text{HF}}^2}{30} J(J_{\text{ex}} - \omega_E - \omega_N) + \frac{[\Delta_{\Delta\text{HF}}^2 + 4\aleph_{\Delta\text{G},\Delta\text{G}+\Delta\text{HF}}]}{120} J(J_{\text{ex}} - \omega_E) + \frac{[\Delta_{\Delta\text{HF}}^2 + 4\aleph_{\Delta\text{G},\Delta\text{G}+\Delta\text{HF}}]}{120} J(J_{\text{ex}} + \omega_E) + \dots \quad (6)$$

For the  $\hat{T}_{+1,\alpha/\beta}$  states these were:

$$-R[\hat{T}_{+1,\beta}] = \frac{\Delta_{\Delta\text{HF}}^2}{180} J(J_{\text{ex}} + \omega_E - \omega_N) + \frac{[\Delta_{\Delta\text{HF}}^2 + 4\aleph_{\Delta\text{G},\Delta\text{G}-\Delta\text{HF}}]}{120} J(J_{\text{ex}} + \omega_E) + \dots \quad (7)$$

and

$$-R[\hat{T}_{+1,\alpha}] = \frac{\Delta_{\Delta\text{HF}}^2}{30} J(J_{\text{ex}} + \omega_E + \omega_N) + \frac{[\Delta_{\Delta\text{HF}}^2 + 4\aleph_{\Delta\text{G},\Delta\text{G}+\Delta\text{HF}}]}{120} J(J_{\text{ex}} + \omega_E) + \dots \quad (8)$$

For the  $\hat{T}_{0,\alpha/\beta}$ , the self-relaxation rates are:

$$-R[\hat{T}_{0,\beta}] = \frac{\Delta_{\text{CSA}}^2}{15} J(\omega_N) + \dots \quad (9)$$

and

$$-R[\hat{T}_{0,\alpha}] = \frac{\Delta_{\text{CSA}}^2}{15} J(\omega_N) + \dots \quad (10)$$

and for  $\hat{T}_{-1,\alpha/\beta}$  the self-relaxation rates:

$$-R[\hat{T}_{-1,\beta}] = \frac{\Delta_{\Delta\text{HF}}^2}{30} J(J_{\text{ex}} - \omega_E - \omega_N) + \frac{[\Delta_{\Delta\text{HF}}^2 + 4\aleph_{\Delta\text{G},\Delta\text{G}-\Delta\text{HF}}]}{120} J(J_{\text{ex}} - \omega_E) + \dots \quad (11)$$

and

$$-R[\hat{T}_{-1,\alpha}] = \frac{\Delta_{\Delta\text{HF}}^2}{180} J(J_{\text{ex}} - \omega_E + \omega_N) + \frac{[\Delta_{\Delta\text{HF}}^2 + 4\aleph_{\Delta\text{G},\Delta\text{G}+\Delta\text{HF}}]}{120} J(J_{\text{ex}} - \omega_E) + \dots \quad (12)$$

where  $\Delta\mathbf{G} = \mathbf{G}_1 - \mathbf{G}_2$  and  $\Delta\mathbf{HF} = \mathbf{HFC}_1 - \mathbf{HFC}_2$  are anisotropies associated to the differences between the two g- and electron/nuclear hyperfine coupling tensors, respectively;  $\text{CSA}$  is the chemical shift anisotropy tensor; and, as is usual in spin relaxation theory,<sup>22,23</sup> all rates contain combinations of second-rank norms squared  $\Delta_{\mathbf{A}}^2$  for all the aforementioned tensors  $\mathbf{A}$ ,<sup>42</sup> and second-rank scalar products  $\aleph_{\mathbf{A},\mathbf{B}}$  of tensors  $\mathbf{A}$  and  $\mathbf{B}$ , as defined in Supporting Information 5. The "..." in Eqs. (5)-(12) denote terms that contribute equally to  $\hat{\rho}_\alpha$  and  $\hat{\rho}_\beta$  and thus are not relevant for the J-DNP effect; full analytical expressions for all the self-relaxation rates are given in Supporting Information 4. As mentioned, for normal liquids and high  $B_0$  fields  $J(\omega_E) \approx 0$ ; *i.e.*, most contributions to the rates in Eqs. (5) - (12) can be disregarded.

Exceptions, however, will arise when a spectral density's  $\omega$ -argument is  $\omega_N$ , or when it can be made zero by  $J_{ex}$ . Under such conditions large differences arise between the self-relaxation rates of the  $\hat{O}_\alpha$  and  $\hat{O}_\beta$  population operators, leading to the transient generation of non-zero  $\hat{N}_Z \hat{S}_0$ ,  $\hat{N}_Z \hat{T}_{\pm 1}$  states. This can be most easily appreciated for  $\hat{S}_{0,\alpha}$  and  $\hat{S}_{0,\beta}$  relaxation rates: the latter will be dominated by the  $J(J_{ex} + \omega_E + \omega_N)$  term if  $J_{ex} = -(\omega_E + \omega_N)$ , and the former by the  $J(J_{ex} - \omega_E - \omega_N)$  if  $J_{ex} = +(\omega_E + \omega_N)$ . In either case, such  $J_{ex}$  condition will result in large differences between  $R[\hat{O}_\alpha]$  and  $R[\hat{O}_\beta]$  due to the cancellation of  $\omega_E$  by  $J_{ex}$ . Similar differences can be observed in Figure 5 also for  $\hat{T}_{\pm 1,\alpha}$  and  $\hat{T}_{\pm 1,\beta}$ .

#### 4. Conclusions and outlook

The present study introduced a new proposal for enhancing signals in solution state NMR that could potentially provide substantial sensitivity gains for a wide range of magnetic fields and rotational correlation times. This J-DNP mechanism uses biradicals, it is transient, and it emerges in the hitherto unexplored  $J_{ex} = \pm(\omega_E + \omega_N)$  regimes. This requires exchange couplings in the order of the electron Larmor frequencies, which range between 196 GHz and 658 GHz for NMR measurements between 7 T and 23.5 T; such values are not out of the ordinary, and have been reported in the literature.<sup>21-23</sup>

Under such conditions, both numerical and analytical simulations provide coinciding predictions of significant NMR polarization build-ups. These enhancements require irradiation times lasting a fraction of a second and, if implemented at the right frequency, they can proceed efficiently with microwave nutation fields  $\leq 1$  MHz (see Supporting information 1 for additional details). Supporting Information 6 demonstrates that similar enhancements are reached with zero  $g$ - and shielding tensor anisotropies; the enhancements are also preserved if the two electrons have different but isotropic  $g$ -tensors. Much like the radical pair mechanism of CIDNP, the mechanism of J-DNP requires different hyperfine coupling to the two electrons; this drives nuclear state dependent electron relaxation which disappears if the nucleus is symmetrically placed between the two electrons. The enhancement is also quenched if the two electrons have different anisotropic  $g$ -tensors – the resulting electron relaxation would, at high magnetic fields, overtake the weaker differential relaxation mechanism. Likewise, the enhancement goes to zero if the nucleus remains too distant from the biradical: for instance, a proton placed 20 Å away from the biradical may require over 1 s to achieve significant polarization gains – a time by which the DNP effect will lose against competing relaxation pathways.

Despite its encouraging conclusions, the present study also made a number of strong assumptions. It assumes that the non-Redfield relaxation terms in monoradicals resembled those acting in biradicals (Supporting Information 1); it remains to be seen how realistic this assumption is. Another major approximation was assuming a fixed electron/electron/nuclear geometry over the course of the DNP process: as the latter requires 10-100 ms and molecules in regular liquids diffuse tens of microns over such times, this fixed molecular geometry assumption is clearly unrealistic. On the other hand, a similar fixed-geometry assumption is successfully used and leads to realistic predictions in Overhauser DNP, where it works by virtue of DNP's independence on maintaining specific cross-correlations (a requirement present in our previous CCDNP proposal). Likewise, we hypothesize that the different  $R[\hat{O}_{\alpha/\beta}]$  rates required for J-DNP will be preserved regardless of the transient contact that a specific nucleus makes with an ensemble of biradicals over the course of its spin polarization process. Experiments are in progress to evaluate the correctness of these assumptions.

## 5. Acknowledgments

This project was funded by the Weizmann-UK Joint Research Programme, the Israel Science Foundation (ISF 965/18), the Perlman Family Foundation, and the US National Science Foundation (grants numbers CHE-1808660, DMR-1644779). MGC acknowledges Weizmann's Faculty of Chemistry for a Dean Fellowship. LF holds the Bertha and Isadore Gudelsky Professorial Chair and Heads the Clore Institute for High-Field Magnetic Resonance Imaging and Spectroscopy, whose support is acknowledged.

## 6. Author contribution

LF and MGC discovered the J-DNP effect and, jointly with IK, provided a theoretical description of its mechanism. IK has written Spinach kernel code and the symbolic processing engine, MGC wrote the simulation scripts to perform analytical and numerical simulations, and derived the analytical expressions of the relaxation rates. All authors discussed and wrote the paper.

## 7. Competing interests

The authors declare no competing interests.

## 8. References

- 1 Overhauser, A. W. Polarization of nuclei in metals. *Physical Review* **92**, 411 (1953).
- 2 Carver, T. R. & Slichter, C. P. Experimental verification of the Overhauser nuclear polarization effect. *Physical Review* **102**, 975 (1956).
- 3 Hu, K.-N., Yu, H.-h., Swager, T. M. & Griffin, R. G. Dynamic nuclear polarization with biradicals. *Journal of the American Chemical Society* **126**, 10844 (2004).
- 4 Bajaj, V. S. *et al.* 250 GHz CW gyrotron oscillator for dynamic nuclear polarization in biological solid state NMR. *Journal of Magnetic Resonance* **189**, 251 (2007).
- 5 Bajaj, V. *et al.* Dynamic nuclear polarization at 9 T using a novel 250 GHz gyrotron microwave source. *Journal of Magnetic Resonance* **213**, 404 (2011).
- 6 Hu, K. N., Debelouchina, G. T., Smith, A. A. & Griffin, R. G. Quantum mechanical theory of dynamic nuclear polarization in solid dielectrics. *The Journal of Chemical Physics* **134**, 125105, doi:10.1063/1.3564920 (2011).
- 7 Ardenkjaer-Larsen, J. H. *et al.* Increase in signal-to-noise ratio of > 10,000 times in liquid-state NMR. *Proceedings of the National Academy of Sciences of the USA* **100**, 10158, doi:10.1073/pnas.1733835100 (2003).
- 8 Golman, K., Lerche, M., Pehrson, R. & Ardenkjaer-Larsen, J. H. Metabolic imaging by hyperpolarized <sup>13</sup>C magnetic resonance imaging for in vivo tumor diagnosis. *Cancer research* **66**, 10855 (2006).
- 9 Dubroca, T., Wi, S., van Tol, J., Frydman, L. & Hill, S. Large volume liquid state scalar Overhauser dynamic nuclear polarization at high magnetic field. *Physical Chemistry Chemical Physics* **21**, 21200, doi:10.1039/c9cp02997d (2019).
- 10 Parigi, G., Ravera, E., Bennati, M. & Luchinat, C. Understanding Overhauser Dynamic Nuclear Polarisation through NMR relaxometry. *Mol Phys* **117**, 888, doi:10.1080/00268976.2018.1527409 (2019).
- 11 Levien, M., Hiller, M., Tkach, I., Bennati, M. & Orlando, T. Nitroxide Derivatives for Dynamic Nuclear Polarization in Liquids: The Role of Rotational Diffusion. *The Journal of Physical Chemistry Letters* **11**, 1629, doi:10.1021/acs.jpcllett.0c00270 (2020).
- 12 Loening, N. M., Rosay, M., Weis, V. & Griffin, R. G. Solution-state dynamic nuclear polarization at high magnetic field. *Journal of the American Chemical Society* **124**, 8808, doi:10.1021/ja026660g (2002).

- 13 Liu, G. Q. *et al.* One-thousand-fold enhancement of high field liquid nuclear magnetic resonance signals at room temperature. *Nature Chemistry* **9**, 676-680, doi:10.1038/Nchem.2723 (2017).
- 14 Hausser, K. H. & Stehlik, D. in *Advances in Magnetic and Optical Resonance* Vol. 3 79 (Elsevier, 1968).
- 15 Griesinger, C. *et al.* Dynamic nuclear polarization at high magnetic fields in liquids. *Progress in Nuclear Magnetic Resonance Spectroscopy* **64**, 4, doi:<https://doi.org/10.1016/j.pnmrs.2011.10.002> (2012).
- 16 Prisner, T., Denysenkov, V. & Sezer, D. Liquid state DNP at high magnetic fields: Instrumentation, experimental results and atomistic modelling by molecular dynamics simulations. *Journal of Magnetic Resonance* **264**, 68, doi:<https://doi.org/10.1016/j.jmr.2015.11.004> (2016).
- 17 Ravera, E., Luchinat, C. & Parigi, G. Basic facts and perspectives of Overhauser DNP NMR. *Journal of Magnetic Resonance* **264**, 78 (2016).
- 18 Concilio, M. G., Soundararajan, M., Frydman, L. & Kuprov, I. High-field solution state DNP using cross-correlations. *Journal of Magnetic Resonance* **326**, 106940, doi:ARTN 106940 10.1016/j.jmr.2021.106940 (2021).
- 19 Reginsson, G. W., Kunjir, N. C., Sigurdsson, S. T. & Schiemann, O. Trityl radicals: spin labels for nanometer-distance measurements. *Chemistry* **18**, 13580, doi:10.1002/chem.201203014 (2012).
- 20 Jassoy, J. J., Meyer, A., Spicher, S., Wuebben, C. & Schiemann, O. Synthesis of Nanometer Sized Bis- and Tris-trityl Model Compounds with Different Extent of Spin-Spin Coupling. *Molecules* **23**, 682, doi:ARTN 682 10.3390/molecules23030682 (2018).
- 21 Fleck, N. *et al.* C-C Cross-Coupling Reactions of Trityl Radicals: Spin Density Delocalization, Exchange Coupling, and a Spin Label. *J Org Chem* **84**, 3293-3303, doi:10.1021/acs.joc.8b03229 (2019).
- 22 Redfield, A. in *Advances in Magnetic and Optical Resonance* Vol. 1 1 (Elsevier, 1965).
- 23 Goldman, M. Formal theory of spin-lattice relaxation. *J Magn Reson* **149**, 160, doi:10.1006/jmre.2000.2239 (2001).
- 24 Kuprov, I., Wagner-Rundell, N. & Hore, P. Bloch-Redfield-Wangsness theory engine implementation using symbolic processing software. *Journal of Magnetic Resonance* **184**, 196 (2007).
- 25 Kuprov, I. Diagonalization-free implementation of spin relaxation theory for large spin systems. *Journal of Magnetic Resonance* **209**, 31 (2011).
- 26 Goodwin, D. & Kuprov, I. Auxiliary matrix formalism for interaction representation transformations, optimal control, and spin relaxation theories. *The Journal of chemical physics* **143**, 084113 (2015).
- 27 Bargon, J., Fischer, H. & Johnsen, U. Kernresonanz-Emissionslinien während rascher Radikalreaktionen. *Zeitschrift für Naturforschung A* **22**, 1551 (1967).
- 28 Kaptein, R. & Oosterhoff, L. J. Chemically induced dynamic nuclear polarization II: (Relation with anomalous ESR spectra). *Chem. Phys. Lett.* **4**, 195 (1969).
- 29 Closs, G. L. Mechanism explaining nuclear spin polarizations in radical combination reactions. *J. Am. Chem. Soc.* **93**, 1546 (1971).
- 30 Santabarbara, S. *et al.* Bidirectional electron transfer in photosystem I: determination of two distances between P700+ and A1- in spin-correlated radical pairs. *Biochemistry* **44**, 2119, doi:10.1021/bi048445d (2005).
- 31 Ardenkjaer-Larsen, J. H. *et al.* EPR and DNP properties of certain novel single electron contrast agents intended for oximetric imaging. *Journal of Magnetic Resonance* **133**, 1, doi:DOI 10.1006/jmre.1998.1438 (1998).

- 32 Yong, L. *et al.* Electron spin relaxation of triarylmethyl radicals in fluid solution. *J Magn Reson* **152**, 156, doi:10.1006/jmre.2001.2379 (2001).
- 33 Owenius, R., Eaton, G. R. & Eaton, S. S. Frequency (250 MHz to 9.2 GHz) and viscosity dependence of electron spin relaxation of triarylmethyl radicals at room temperature. *Journal of Magnetic Resonance* **172**, 168, doi:10.1016/j.jmr.2004.10.007 (2005).
- 34 Hogben, H., Krzystyniak, M., Charnock, G., Hore, P. & Kuprov, I. Spinach - a software library for simulation of spin dynamics in large spin systems. *Journal of Magnetic Resonance* **208**, 179 (2011).
- 35 Hore, P. J. & Broadhurst, R. W. Photo-CIDNP of biopolymers. *Prog. NMR Spectrosc.* **25**, 345 (1993).
- 36 Wangsness, R. K. & Bloch, F. The dynamical theory of nuclear induction. *Physical Review* **89**, 728 (1953).
- 37 Levitt, M. H. & Di Bari, L. Steady state in magnetic resonance pulse experiments. *Phys Rev Lett* **69**, 3124-3127, doi:10.1103/PhysRevLett.69.3124 (1992).
- 38 Kuprov, I. *et al.* Anomalous Nuclear Overhauser Effects in Carbon-Substituted Aziridines: Scalar Cross-Relaxation of the First Kind. *Angewandte Chemie International Edition* **54**, 3697 (2015).
- 39 Kuprov, I., Craggs, T. D., Jackson, S. E. & Hore, P. J. Spin relaxation effects in photochemically induced dynamic nuclear polarization spectroscopy of nuclei with strongly anisotropic hyperfine couplings. *Journal of the American Chemical Society* **129**, 9004-9013, doi:10.1021/ja0705792 (2007).
- 40 Müller-Warmuth, W., Vilhjalmsson, R., Gerlof, P., J., S. & Trommel, J. Intermolecular interactions of benzene and carbon tetrachloride with selected free radicals in solution as studied by <sup>13</sup>C and <sup>1</sup>H dynamic nuclear polarization. *Mol. Phys.* **31**, 1055–1067 (1976).
- 41 Levien, M. *et al.* Spin density localization and accessibility of organic radicals affect liquid-state DNP efficiency. *Physical Chemistry Chemical Physics* **23**, 4480-4485, doi:10.1039/d0cp05796g (2021).
- 42 Blicharski, J. Nuclear magnetic relaxation by anisotropy of the chemical shift. *Z Naturforsch Pt A* **27**, 1456 (1972).
- 43 Vega, S. Fictitious spin 1/2 operator formalism for multiple quantum NMR. *J. Chem. Phys.* **68**, 5518 (1978).
- 44 Ernst, R., R.; Bodenhausen, G.; Wokaun, A. . *Principles of Nuclear Magnetic Resonance in One and Two Dimensions*. 610 (Clarendon Press (Oxford Oxfordshire and New York), 1987).
- 45 Pileio, G. Singlet NMR methodology in two-spin-1/2 systems. *Prog Nucl Magn Reson Spectrosc* **98-99**, 1, doi:10.1016/j.pnmrs.2016.11.002 (2017).
- 46 Bengs, C. & Levitt, M. H. SpinDynamica: Symbolic and numerical magnetic resonance in a Mathematica environment. *Magn Reson Chem* **56**, 374-414, doi:10.1002/mrc.4642 (2018).

# Supplementary Information for

## *J*-driven Dynamic Nuclear Polarization for sensitizing high field solution state NMR

*Maria Grazia Concilio*<sup>1\*</sup>, *Ilya Kuprov*<sup>2</sup>, *Lucio Frydman*<sup>1,3\*</sup>

<sup>1</sup>Department of Chemical and Biological Physics, Weizmann Institute of Science, Rehovot, Israel.

<sup>2</sup>School of Chemistry, University of Southampton, Southampton, UK.

<sup>3</sup>National High Magnetic Field Laboratory, Tallahassee, Florida, USA.

### Supporting Information 1: $R_1/R_2$ relaxation rate analysis for mono- and bis-trityl radicals

As this is a purely theoretical study, we consider it necessary to test our numerical simulations against experimental measurements. Given the paucity of solution-state NMR data about relaxation rates in biradicals, theoretical models were used to estimate electron longitudinal and transverse relaxation rates for trityl monoradicals – for which solution-state measurements have been reported in <sup>32,33</sup>. Following the treatment in <sup>33</sup>, electron  $R_1$  rate for this radical will be assumed to have three contributions:

$$\begin{aligned} R_{1,\text{total}} &= R_{1,\text{local}} + R_{1,\text{BRW}} + R_{1,\text{solvent}} \\ &\approx R_{1,\text{local}} + R_{1,\text{BRW}} \end{aligned} \quad (\text{S1a})$$

Here  $R_{1,\text{local}}$  is the self-relaxation rate arising from the local vibrational modes related to the stretching of bonds in the radical, and is a magnetic field independent contribution estimated by Eaton et al <sup>33</sup> as  $5.9 \times 10^4$  Hz for per-deutero and  $6.1 \times 10^4$  Hz for per-protio trityls. The Redfield component:

$$R_{1,\text{BRW}} = n \left[ \underbrace{\left( \frac{\Delta_{\text{HF,intra}}^2}{9} \right) \left( \frac{\tau_c}{(1 + \tau_c^2 \omega_E^2)} \right)}_{\text{hyperfine relaxation}} \right] + \underbrace{\left( \frac{2\Delta_G^2}{15} \right) \left( \frac{\tau_c}{(1 + \tau_c^2 \omega_E^2)} \right)}_{\text{g-anisotropy relaxation}} \quad (\text{S1b})$$

is the relaxation rate which arises from the stochastic modulation of the radical's  $g$ -tensor anisotropy and of the hyperfine interactions between the electron and the  $n$  protons interacting with it within the radical (that in the case of a trityl monomer can be considered approximately the same); this is the kind of rate computed in the main text based on Bloch-Redfield-Wangsness theory in terms of  $\Delta_G^2$  and  $\Delta_{\text{HF,intra}}^2$  coupling strengths; i.e., of the second-rank norm Blicharsky squared,<sup>42</sup> already mentioned in the main text and defined in Eq. S58 in Supporting Information 5, for the  $g$ -anisotropy and the hyperfine interaction tensors. Finally,

$$R_{1,\text{solvent}} = n_{\text{solv}} \left[ \left( \frac{\Delta_{\text{HF,inter}}^2}{9} \right) \left( \frac{\tau_{\text{solv}}}{(1 + \tau_{\text{solv}}^2 \omega_E^2)} \right) \right] \quad (\text{S1c})$$

is an *ad hoc* relaxation term, arising from the dipolar interaction between the electron and  $n_{\text{solv}}$  solvent molecules; the coupling strength of this relaxation is given by the second-rank norm squared of the dipolar interaction tensor between the electron and the solvent protons  $\Delta_{\text{HF,inter}}^2$ , and by a

correlation time  $\tau_{\text{solvent}}$ . Eaton et al in <sup>33</sup> have estimated the  $R_{1,\text{solvent}}$  in Eq. (S1c) as  $\tau_{\text{solvent}} = F \tau_C$ , where  $F$  is a ratio between the solvent correlation time and the trityl correlation time, that is different for each radical. As this latter term is much smaller than the remaining relaxation rates it is henceforth ignored in both the mono- and bi-radical estimations. Finally, in a non-viscous solvent, the  $R_{2,\text{total}}$  corresponds to  $R_{1,\text{total}} + R_{2,\text{BRW}}$  <sup>33</sup>. The BRW theory predicts this second term to be:

$$R_{2,\text{BRW}} = n \left[ \underbrace{\left( \frac{\Delta_{\text{HF, trityl}}^2}{90} \right) \left( 2 + \frac{5\tau_C}{(1 + \tau_C^2 \omega_E^2)} + \frac{3\tau_C}{(1 + \tau_C^2 \omega_N^2)} \right)}_{\text{hyperfine relaxation}} \right] + \underbrace{\left( \frac{\Delta_G^2}{45} \right) \left( 4 + \frac{3\tau_C}{(1 + \tau_C^2 \omega_E^2)} \right)}_{\text{g-anisotropy relaxation}} \quad (\text{S2})$$

Table S1 compares the  $R_{1,\text{total}}$  and  $R_{2,\text{total}}$  values determined from Eqs. (S1a) and (S2), with values reported experimentally in <sup>33</sup> for per-protio and per-deutero trityls at different fields. There is good agreement between both sets. Notice, however, that the low magnetic fields explored in this comparison, it is the local vibrational modes contributing to  $R_{1,\text{local}}$  that dominate the longitudinal- and transverse relaxation rates. As this parameter was estimated from the experimental data, the good agreement is not surprising.

**Table S1:** Comparison between  $T_1$  and  $T_2$  calculated using Eq. (S1a) and Eq. (S2) and experimental  $T_1$  and  $T_2$  in water for trityl- $\text{CD}_3$  and trityl- $\text{CH}_3$  obtained from <sup>33</sup>.  $n$  represents the number of trityl protons dipole-coupled to the radical. For trityl- $\text{CH}_3$ , the distances between the electron and all 36 protons in the radical were set equal to 5.3 Å.

Magnetic field / T	$R_1$ from Eq. 1 / Hz	Experimental $R_1$ / Hz	$R_2$ from Eq. 2 / Hz	Experimental $R_2$ / Hz
<b>Trityl-<math>\text{CD}_3</math> radical, <math>n = 0</math>, <math>R_{1,\text{local}} = 0.59 \times 10^5</math> Hz</b>				
<b>0.33 T (X-band)</b>	$5.9 \times 10^4$	$5.9 \times 10^4$	$6.7 \times 10^4$	$9.1 \times 10^4$
<b>0.11 T (S-band)</b>	$5.9 \times 10^4$	$6.2 \times 10^4$	$6.2 \times 10^4$	$8.3 \times 10^4$
<b>0.03 T (L-band)</b>	$5.9 \times 10^4$	$7.2 \times 10^4$	$6.2 \times 10^4$	$8.3 \times 10^4$
<b><math>9 \times 10^{-3}</math> T (250 MHz)</b>	$6.2 \times 10^4$	/	$6.2 \times 10^4$	$9.1 \times 10^4$
<b>Trityl-<math>\text{CH}_3</math> radical <math>\rightarrow n = 36</math>, <math>R_{1,\text{local}} = 0.61 \times 10^5</math> Hz</b>				
<b>0.33 T (X-band)</b>	$6.2 \times 10^4$	$6.2 \times 10^4$	$2.3 \times 10^5$	$1.1 \times 10^5$
<b>0.11 T (S-band)</b>	$6.6 \times 10^4$	$7.1 \times 10^4$	$1.0 \times 10^5$	$1.1 \times 10^5$
<b>0.03 T (L-band)</b>	$8.3 \times 10^4$	$8.3 \times 10^4$	$1.1 \times 10^5$	$1.1 \times 10^5$
<b><math>9 \times 10^{-3}</math> T (250 MHz)</b>	$9.1 \times 10^4$	/	$1.3 \times 10^5$	$1.3 \times 10^5$

It is enlightening to extend this monoradical analysis to the case of trityl bi-radicals. In this case it is reasonable to assume that the contributions coming from solvent-induced and bond-vibration-induced terms to  $R_1$  relaxation, will remain similar as those given in Table S1. The electron  $R_{1,\text{BRW}}$  and  $R_{2,\text{BRW}}$  longitudinal and transverse rates, however, will be significantly increased by the electron-electron dipolar interaction, and will now be dominated by  $J(0)$ -containing terms that depend on the rotational correlation time but are independent of the magnetic field. A full analysis of these two terms using symbolic processing software <sup>24</sup> leads to:

$$\begin{aligned}
R_{1,\text{BRW}} = -R[\hat{E}_Z] &= \frac{\Delta_{\text{EE}}^2}{90} J(0) + \frac{\aleph_{(\text{HFC},\Sigma\text{HF}),\text{inter}}}{18} J(\omega_{\text{E}}) + \\
&+ \frac{\aleph_{(\text{HFC},\Delta\text{HF}),\text{inter}}}{360} \left[ 3J(J_{\text{ex}} + \omega_{\text{E}}) + 3J(J_{\text{ex}} - \omega_{\text{E}}) + 6J(J_{\text{ex}} + \omega_{\text{E}} + \omega_{\text{N}}) + \right. \\
&\left. + 6J(J_{\text{ex}} - \omega_{\text{E}} - \omega_{\text{N}}) + J(J_{\text{ex}} + \omega_{\text{E}} - \omega_{\text{N}}) + J(J_{\text{ex}} - \omega_{\text{E}} + \omega_{\text{N}}) \right] + \\
&+ \text{n} \left( \frac{\aleph_{(\text{HFC},\Sigma\text{HF}),\text{intra}}}{18} J(\omega_{\text{E}}) + \right. \\
&\left. \frac{\aleph_{(\text{HFC},\Delta\text{HF}),\text{intra}}}{360} \left[ 3J(J_{\text{ex}} + \omega_{\text{E}}) + 3J(J_{\text{ex}} - \omega_{\text{E}}) + 6J(J_{\text{ex}} + \omega_{\text{E}} + \omega_{\text{N}}) + \right. \right. \\
&\left. \left. + 6J(J_{\text{ex}} - \omega_{\text{E}} - \omega_{\text{N}}) + J(J_{\text{ex}} + \omega_{\text{E}} - \omega_{\text{N}}) + J(J_{\text{ex}} - \omega_{\text{E}} + \omega_{\text{N}}) \right] \right) + \\
&+ \frac{[4\aleph_{\text{G},\Delta\text{G}} + 2\aleph_{\text{EE},-\Delta\text{G}}]}{120} J(J_{\text{ex}} - \omega_{\text{E}}) + \frac{[4\aleph_{\text{G},\Delta\text{G}} + 2\aleph_{\text{EE},\Delta\text{G}}]}{120} J(J_{\text{ex}} + \omega_{\text{E}}) + \\
&+ \frac{[3\Delta_{\text{EE}}^2 + 6\aleph_{\text{G},\Sigma\text{G}}]}{90} J(\omega_{\text{E}}) + \frac{\Delta_{\text{EE}}^2}{15} J(2\omega_{\text{E}})
\end{aligned} \tag{S3}$$

and

$$\begin{aligned}
R_{2,\text{BRW}} = -R[\hat{E}_+] &= \frac{\Delta_{\text{EE}}^2}{36} J(0) + \frac{4\aleph_{\text{G},\Sigma\text{G}}}{90} J(0) + \\
&+ \frac{\aleph_{(\text{HFC},\Sigma\text{HF}),\text{inter}}}{90} J(0) + \frac{\aleph_{(\text{HFC},\Sigma\text{HF}),\text{inter}}}{120} J(\omega_{\text{N}}) + \frac{\aleph_{(\text{HFC},\Sigma\text{HF}),\text{inter}}}{36} J(\omega_{\text{E}}) + \\
&+ \frac{\aleph_{(\text{HFC},\Delta\text{HF}),\text{inter}}}{720} \left[ 3J(J_{\text{ex}} - \omega_{\text{E}}) + 3J(J_{\text{ex}} + \omega_{\text{E}}) + 12J(J_{\text{ex}} - \omega_{\text{E}} - \omega_{\text{N}}) + 12J(J_{\text{ex}} + \omega_{\text{E}} - \omega_{\text{N}}) + \right. \\
&\left. + J(J_{\text{ex}} - \omega_{\text{E}} + \omega_{\text{N}}) + 6J(J_{\text{ex}} + \omega_{\text{N}}) + 6J(J_{\text{ex}} + \omega_{\text{E}} + \omega_{\text{N}}) \right] + \\
&+ \text{n} \left( \frac{\aleph_{(\text{HFC},\Sigma\text{HF}),\text{intra}}}{90} J(0) + \frac{\aleph_{(\text{HFC},\Sigma\text{HF}),\text{intra}}}{120} J(\omega_{\text{N}}) + \frac{\aleph_{(\text{HFC},\Sigma\text{HF}),\text{intra}}}{36} J(\omega_{\text{E}}) + \right. \\
&\left. + \frac{\aleph_{(\text{HFC},\Delta\text{HF}),\text{intra}}}{720} \left[ 3J(J_{\text{ex}} - \omega_{\text{E}}) + 3J(J_{\text{ex}} + \omega_{\text{E}}) + 12J(J_{\text{ex}} - \omega_{\text{E}} - \omega_{\text{N}}) + 12J(J_{\text{ex}} + \omega_{\text{E}} - \omega_{\text{N}}) + \right. \right. \\
&\left. \left. + J(J_{\text{ex}} - \omega_{\text{E}} + \omega_{\text{N}}) + 6J(J_{\text{ex}} + \omega_{\text{N}}) + 6J(J_{\text{ex}} + \omega_{\text{E}} + \omega_{\text{N}}) \right] \right) + \\
&+ \frac{[4\aleph_{\text{G},\Delta\text{G}} + 2\aleph_{\text{EE},\Delta\text{G}}]}{240} J(J_{\text{ex}} - \omega_{\text{E}}) + \frac{[4\aleph_{\text{G},\Delta\text{G}} + 2\aleph_{\text{EE},-\Delta\text{G}}]}{240} J(J_{\text{ex}} + \omega_{\text{E}}) + \\
&+ \frac{[9\Delta_{\text{EE}}^2 + 6\aleph_{\text{G},\Sigma\text{G}}]}{180} J(\omega_{\text{E}}) + \frac{\Delta_{\text{EE}}^2}{30} J(2\omega_{\text{E}})
\end{aligned} \tag{S4}$$

where the symbols are as described in the Supplementary Information 5, and we have made a distinction between hyperfine couplings with  $n$  protons within the biradical (“intra”), and with one proton that belongs to the solvent (“inter”) and could be a target of Overhauser DNP (ODNP). At the fields of interest in our studies, all spectral densities that have the electron and the nuclear Larmor frequency in them can be disregarded. This leaves solely the terms involving zero-frequency spectral densities:

$$R_{1,\text{BRW}} = -R[\hat{E}_Z] \simeq \frac{\Delta_{\text{EE}}^2}{90} J(0) \tag{S5}$$

and

$$R_{2,\text{BRW}} = -R[\hat{E}_+] = \frac{\Delta_{\text{EE}}^2}{36} J(0) + \frac{4\aleph_{\text{G},\Sigma\text{G}}}{90} J(0) + \frac{\aleph_{(\text{HFC},\Sigma\text{HF}),\text{inter}}}{90} J(0) + \text{n} \left( \frac{\aleph_{(\text{HFC},\Sigma\text{HF}),\text{intra}}}{90} J(0) \right) \tag{S6}$$

$R_{1,\text{BRW}}$  is thus dominated by  $\Delta_{\text{EE}}^2$ , i.e., by the dipolar interaction between electrons; and  $R_{2,\text{BRW}}$  is dominated by this term as well as by the second rank scalar products  $\aleph_{\text{G},\Sigma\text{G}}$  and  $\aleph_{\text{HFC},\Sigma\text{HF}}$  between the  $g$ -

tensor of one electron and the sum of the two  $g$ -tensors, and by the hyperfine coupling between one electron and one proton, and the sum of the hyperfines of the two electrons and one proton, respectively. The magnitudes of the coefficients in Eq. (S3) and Eq. (S4) for the case of a bistrityl-type biradical, are shown in the Table S2. These coefficients will scale according to spectral densities; Figure S1 show how these BRW-derived  $R_1$  and  $R_2$  terms change with the biradical's correlation time  $\tau_c$ . These rates should be compared with the relaxivity contributions arising from the vibrational local modes, which are likely to be in the order of what they were for the monotrityl radical i.e.,  $\approx 5 \cdot 10^4$  Hz. It follows that for the trityl bis-radical the contribution of these  $R_{1,local}$  will no longer be dominant, primarily due to the onset of relaxation effects driven by  $\Delta_{EE}^2$  and  $\aleph_{G,\Sigma G}$  (the latter mostly at the high fields of interest; Table 1).

**Table S2:** Magnitude of the second-rank norm squared and the scalar products (defined in Supporting Information 5) predicted by Eqs. (S3) and (S6), for a trityl-based biradical with parameters as given in the Table 1.

$\Delta_A^2 / \aleph_{A,B}$	Magnitude / (rad/s) <sup>2</sup>
$\Delta_{EE}^2$	$2 \times 10^{16}$
$\aleph_{G,\Delta G}$	472
$\aleph_{G,\Sigma G}$	$2 \times 10^{17}$
$\aleph_{EE,\Delta G}$ ( $\aleph_{EE,-\Delta G}$ )	687699 / -687699
$\aleph_{(HFC,\Sigma HF),intra} / \aleph_{(HFC,\Sigma HF),inter}^1$	$1.30 \times 10^{13} / 4.9 \times 10^{13}$
$\aleph_{(HFC,\Delta HF),intra} / \aleph_{(HFC,\Delta HF),inter}^1$	$1.34 \times 10^{13} / 5.1 \times 10^{13}$

<sup>1</sup> The intra-molecular dipolar interaction between the electron and the methyl protons in each trityl group of the biradical was computed setting a proton-electron distance equal to 5.3 Å (between the proton and its closest electron; electron/proton hyperfine couplings between the two trityls in the molecule were disregarded). The inter-molecular dipolar interaction between the electron and the solvent was computed setting a proton-electron distance equal to 8.3 Å (again: between the proton and its closest electron only).

Rates do not change also with the increase of the intra-molecular protons  $n$  in Eqs. (S3) - (S6), since the term containing  $\aleph_{(HFC,\Sigma HF),intra}$  remains much smaller than the term containing  $\Delta_{EE}^2$ , Fig. S1.

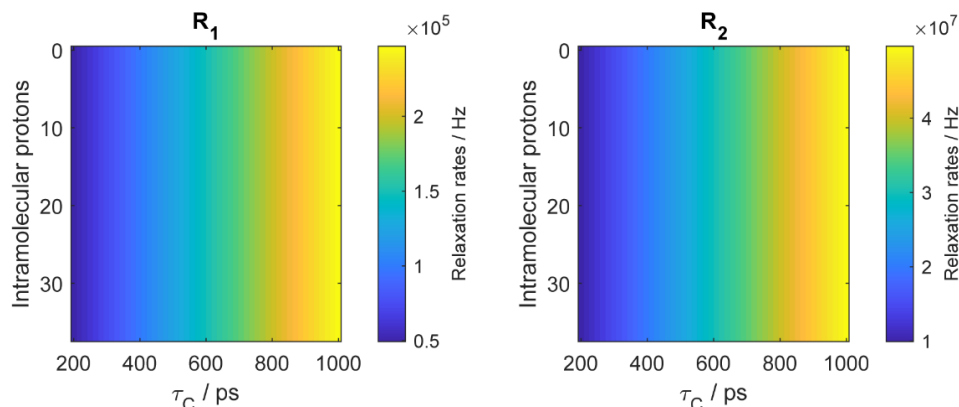


**Fig. S1:**  $R_1$  and  $R_2$  electron relaxation rates predicted by Eq. (S5) and Eq. (S6) as a function of the  $\tau_c$  of the biradical/proton triad and on the number of closest intramolecular protons  $n$  to an electron (36 in the case of a model bis-trityl). For these calculations  $J_{ex}$  was set equal to  $+(\omega_E + \omega_N)$ ,  $B_0$  was set equal to 14.08 T, and other simulation parameters are as given in the Table 1. The absence of a strong dependence with the number of protons reflects the dominant effects of electron-electron dipole and  $g$ -tensor anisotropies on the relaxation processes, over hyperfine counterparts.

It is enlightening to consider how this model predicts the electron saturation and J-DNP enhancement to proceed, as a function of the available microwave power. Considering that the rotational correlation time of the trityl monomer is about 150 ps –calculated from  $\tau_c \approx r_D^2 / D_t$ ,<sup>31</sup> where  $D_t$  is trityl's translational diffusion constant (in the order of  $\sim 10^{-9} \text{ m}^2 \text{ s}^{-1}$ ) and  $r_D$  is the minimum distance approach between an electron in the biradical and a proton in the solvent (estimated at about 5-10 Å)– we decided to set the rotational correlation time for the biradical/proton triad equal to  $\tau_c \approx 500$  ps (close

to what's expected for a trityl biradical). Figure S2 shows the predicted electron saturation and J-DNP enhancement effects expected for this  $\tau_c$  as a function of microwave off-resonance offset and nutation field; similar enhancements and saturation behaviours are predicted for smaller and higher rotational correlation times, up to 1 ns.

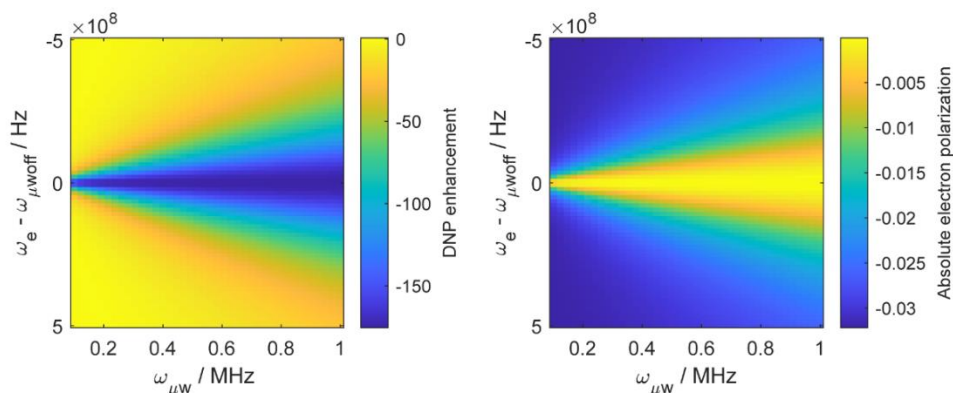


**Fig. S2:** Maximum enhancement (absolute value over the thermal equilibrium) in J-DNP (on the left), achieved between 80-100 ms (depending on the microwave power and  $\Delta\omega$ ), and absolute electron polarization,  $\hat{E}_Z$ , (on the right), as a function of  $\mu\text{W}$  frequency offset from the free electron Larmor frequency and of the  $\mu\text{W}$  nutation power,  $\omega_{\mu\text{W}}$ . For these calculations  $J_{\text{ex}}$  is equal to  $\omega_E + \omega_N$ ,  $B_0$  is 14.08 T,  $\tau_c = 500$  ps for the biradical/proton triad, and other simulation parameters as given in the Table 1.

A comparison between the J-DNP and the Overhauser DNP shows that in the electron/nucleus system, the ODNP case, the enhancement is strong if  $B_0 < 0.5\text{T}$ , but decays to negligible values if  $B_0 \geq 3.4$  T; this is as expected from classical theories<sup>10,11,14-16</sup>, while the transient J-DNP is observed also at  $B_0 \leq 3.4$  T.

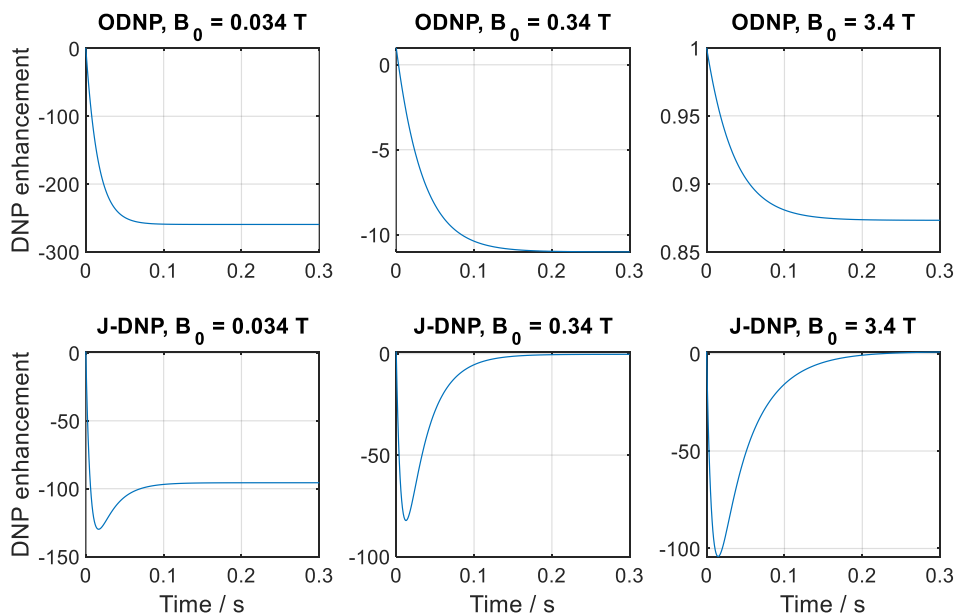


**Fig. S3:** Time domain simulations showing the evolution of the enhancement observed under continuous microwave irradiation of the electrons as a function of  $B_0$ , in ODNP (on the top) and in J-DNP (on the bottom). For ODNP a monoradical with  $\tau_c = 157$  ps (typical of trityl<sup>31</sup>) was assumed; for J-DNP a biradical with  $\tau_c = 500$  ps for the biradical/proton triad and  $J_{\text{ex}} = +(\omega_E + \omega_N)$  was assumed. Other simulation parameters are given in the Table 1.

## Supporting Information 2: The Hamiltonian used in the propagation of the biradical/nuclear system – from the Cartesian to the triplet-singlet representations

The laboratory frame Hamiltonian for a three-spin system composed by two electrons and one proton, where the electrons are connected by dipolar and exchange couplings, and the proton interacts with the electrons through hyperfine (dipolar) coupling only, can be written using single-spin Cartesian operators, as:

$$\hat{H}_{lab.} = \underbrace{\sum_k \hat{E}^{(k)} \cdot \mathbf{Z}_E^{(k)} \cdot \vec{B}_0 + \hat{N} \cdot \mathbf{Z}_N \cdot \vec{B}_0}_{\text{Zeeman interaction}} + \underbrace{\hat{E}^{(1)} \cdot (\mathbf{D} + J_{ex}) \cdot \hat{E}^{(2)}}_{\text{Dipolar and scalar inter-electron interaction}} + \underbrace{\sum_k \hat{E}^{(k)} \cdot \mathbf{A}^{(k)} \cdot \hat{N}}_{\text{Hyperfine interaction}} \quad (S7)$$

where  $\mathbf{Z}_E^{(k)}$  are the Zeeman tensors (including  $g$ -anisotropy) of electron spins  $k=1,2$ ;  $\mathbf{Z}_N$  is the Zeeman tensor of the sole nuclear spin being considered (including the chemical shift anisotropy);  $\mathbf{D}$  is the inter-electron dipolar interaction tensor in the point magnetic dipole approximation;  $J_{ex}$  is the inter-electron scalar (*aka* “exchange”) coupling in angular frequency units;  $\mathbf{A}^{(k)}$  is the hyperfine interaction tensors of the nucleus with the indicated electron  $k$ ;  $\vec{B}_0$  is the external magnetic field; and  $\hat{E}^{(1)}$ ,  $\hat{E}^{(2)}$  and  $\hat{N}$  are the Cartesian spin-1/2 operators for the two electrons and nucleus. A rotating frame transformation with respect to the microwave frequency offset using the operator  $\omega_{\mu\text{woff}} \sum_k \hat{E}_Z^{(k)}$  and preservation of the usual secular and pseudosecular terms, leads to:

$$\begin{aligned} \hat{H}_{rot.} = & \omega_{\Sigma e} (\hat{E}_{1Z} + \hat{E}_{2Z}) + \omega_{\Delta e} (\hat{E}_{1Z} - \hat{E}_{2Z}) + \omega_N \hat{N}_Z + \omega_1 \hat{E}_{1Z} \hat{E}_{2Z} + \omega_2 \left( \frac{\hat{E}_{1+} \hat{E}_{2-} + \hat{E}_{1-} \hat{E}_{2+}}{2} \right) \\ & + A_{\Sigma} (\hat{E}_{1Z} + \hat{E}_{2Z}) \hat{N}_Z + A_{\Delta} (\hat{E}_{1Z} - \hat{E}_{2Z}) \hat{N}_Z + B_{\Sigma} (\hat{E}_{1Z} + \hat{E}_{2Z}) \hat{N}_X + B_{\Delta} (\hat{E}_{1Z} - \hat{E}_{2Z}) \hat{N}_X \end{aligned} \quad (S8)$$

where  $\omega_{\Sigma e}$  and  $\omega_{\Delta e}$  are the sum and the difference between the rotating-frame offsets of the two electrons;  $A_{\Sigma} = A_1 + A_2$  and  $A_{\Delta} = A_1 - A_2$ ;  $B_{\Sigma} = B_1 + B_2$  and  $B_{\Delta} = B_1 - B_2$  are the sum and the difference of the secular and pseudo-secular coefficients describing the hyperfine interaction, respectively; and  $\omega_1 = (J_{ex} + 2\mathbf{D})$  and  $\omega_2 = (J_{ex} - \mathbf{D})$ , where  $\mathbf{D}$  is the inter-electron dipolar interaction tensor.

In the  $J_{ex} \gg \omega_{\Delta e}$  case, where  $\omega_{\Delta e} = \omega_{e1} - \omega_{e2}$  is the difference between the Larmor frequency of the two electrons, the electron Zeeman eigenstates  $|\alpha_{e1}\beta_{e2}\rangle$  and  $|\beta_{e1}\alpha_{e2}\rangle$  are no longer eigenfunctions of the spin Hamiltonian. We therefore express the Hamiltonian in the singlet/triplet electron basis sets<sup>4,6</sup>:

$$\left\{ \begin{array}{l} |\hat{T}_{+1}^{(e1e2)}\rangle = |\alpha_{e1}\alpha_{e2}\rangle, \quad |\hat{T}_0^{(e1e2)}\rangle = \frac{1}{\sqrt{2}} (|\beta_{e1}\alpha_{e2}\rangle + |\alpha_{e1}\beta_{e2}\rangle), \\ |\hat{T}_{-1}^{(e1e2)}\rangle = |\beta_{e1}\beta_{e2}\rangle, \quad |\hat{S}_0^{(e1e2)}\rangle = \frac{1}{\sqrt{2}} (|\beta_{e1}\alpha_{e2}\rangle - |\alpha_{e1}\beta_{e2}\rangle) \end{array} \right\} \otimes \{ \alpha_N, \beta_N \} = \left\{ \begin{array}{l} |\hat{S}_0^{(e1e2)}, \alpha\rangle, \quad |\hat{S}_0^{(e1e2)}, \beta\rangle \\ |\hat{T}_0^{(e1e2)}, \alpha\rangle, \quad |\hat{T}_0^{(e1e2)}, \beta\rangle \\ |\hat{T}_{\pm 1}^{(e1e2)}, \alpha\rangle, \quad |\hat{T}_{\pm 1}^{(e1e2)}, \beta\rangle \end{array} \right\} \quad (S9)$$

where the direct product indicates that the  $\{|\alpha_N\rangle, |\beta_N\rangle\}$  Zeeman basis is preserved for the nucleus (proton). The transformation of the three-spin rotating frame Hamiltonian from a Cartesian basis to its singlet/triplet basis can be performed using fictitious spin-1/2 operators.<sup>43,44</sup> Since the addition of a third nuclear spin has to our knowledge not been reported before, we re-express the rotating-frame Hamiltonian in Eq. (S8), as a sum of terms containing direct products of operators acting in the  $\hat{S}_0\hat{T}_0$  and the  $\hat{T}_{+1}\hat{T}_{-1}$  subspaces, with the nuclear Zeeman base. The fictitious spin-1/2 operators that we use in this study to describe the  $\hat{S}_0\hat{T}_0$  and the  $\hat{T}_{+1}\hat{T}_{-1}$  subspaces follow from Vega’s notation for two-spin fictitious operators<sup>45</sup> and were computed using the SpinDynamica software<sup>46</sup>:

$$\begin{aligned}\hat{L}_X^{T_0 S_0, \alpha} &= \frac{1}{2} \left( \left| \hat{T}_0^{(e1, e2)}, \alpha \right\rangle \langle \hat{S}_0^{(e1, e2)}, \alpha \right| + \left| \hat{S}_0^{(e1, e2)}, \alpha \right\rangle \langle \hat{T}_0^{(e1, e2)}, \alpha \right| \\ &= \frac{\hat{E}_{1Z}}{4} - \frac{\hat{E}_{2Z}}{4} + \frac{1}{2} \left( \hat{E}_{1Z} \hat{N}_Z \right) - \frac{1}{2} \left( \hat{E}_{2Z} \hat{N}_Z \right)\end{aligned}\quad (\text{S10})$$

$$\begin{aligned}\hat{L}_X^{T_0 S_0, \beta} &= \frac{1}{2} \left( \left| \hat{T}_0^{(e1, e2)}, \beta \right\rangle \langle \hat{S}_0^{(e1, e2)}, \beta \right| + \left| \hat{S}_0^{(e1, e2)}, \beta \right\rangle \langle \hat{T}_0^{(e1, e2)}, \beta \right| \\ &= \frac{\hat{E}_{1Z}}{4} - \frac{\hat{E}_{2Z}}{4} - \frac{1}{2} \left( \hat{E}_{1Z} \hat{N}_Z \right) + \frac{1}{2} \left( \hat{E}_{2Z} \hat{N}_Z \right)\end{aligned}\quad (\text{S11})$$

which we combine to obtain:

$$\omega_{\Delta e} \left( \hat{E}_{1Z} - \hat{E}_{2Z} \right) = 2\omega_{\Delta e} \left( \hat{L}_X^{T_0 S_0, \alpha} + \hat{L}_X^{T_0 S_0, \beta} \right) \quad (\text{S12})$$

$$A_{\Lambda} \left( \hat{E}_{1Z} \hat{N}_Z - \hat{E}_{2Z} \hat{N}_Z \right) = A_{\Lambda} \left( \hat{L}_X^{T_0 S_0, \alpha} - \hat{L}_X^{T_0 S_0, \beta} \right) \quad (\text{S13})$$

The longitudinal fictitious  $\frac{1}{2}$ -spin operators for the electron in the  $\hat{S}_0 \hat{T}_0$  are:

$$\begin{aligned}\hat{L}_Z^{T_0 S_0, \alpha} &= \frac{1}{2} \left( \left| \hat{T}_0^{(e1, e2)}, \alpha \right\rangle \langle \hat{T}_0^{(e1, e2)}, \alpha \right| - \left| \hat{S}_0^{(e1, e2)}, \alpha \right\rangle \langle \hat{S}_0^{(e1, e2)}, \alpha \right| \\ &= -\frac{1}{2} \hat{E}_{1X} \hat{E}_{2X} - \frac{1}{2} \hat{E}_{1Y} \hat{E}_{2Y} - \hat{E}_{1X} \hat{E}_{2X} \hat{N}_Z - \hat{E}_{1Y} \hat{E}_{2Y} \hat{N}_Z\end{aligned}\quad (\text{S14})$$

$$\begin{aligned}\hat{L}_Z^{T_0 S_0, \beta} &= \frac{1}{2} \left( \left| \hat{T}_0^{(e1, e2)}, \beta \right\rangle \langle \hat{T}_0^{(e1, e2)}, \beta \right| - \left| \hat{S}_0^{(e1, e2)}, \beta \right\rangle \langle \hat{S}_0^{(e1, e2)}, \beta \right| \\ &= -\frac{1}{2} \hat{E}_{1X} \hat{E}_{2X} - \frac{1}{2} \hat{E}_{1Y} \hat{E}_{2Y} + \hat{E}_{1X} \hat{E}_{2X} \hat{N}_Z + \hat{E}_{1Y} \hat{E}_{2Y} \hat{N}_Z\end{aligned}\quad (\text{S15})$$

$$\begin{aligned}\hat{E}^{T_0 S_0, \alpha} &= \left( \left| \hat{T}_0^{(e1, e2)}, \alpha \right\rangle \langle \hat{T}_0^{(e1, e2)}, \alpha \right| + \left| \hat{S}_0^{(e1, e2)}, \alpha \right\rangle \langle \hat{S}_0^{(e1, e2)}, \alpha \right| \\ &= -\hat{E}_{1Z} \hat{E}_{2Z} - 2\hat{E}_{1Z} \hat{E}_{2Z} \hat{N}_Z + \frac{1}{2} \hat{N}_Z + \frac{\mathbf{E}}{4}\end{aligned}\quad (\text{S16})$$

$$\begin{aligned}\hat{E}^{T_0 S_0, \beta} &= \left( \left| \hat{T}_0^{(e1, e2)}, \beta \right\rangle \langle \hat{T}_0^{(e1, e2)}, \beta \right| + \left| \hat{S}_0^{(e1, e2)}, \beta \right\rangle \langle \hat{S}_0^{(e1, e2)}, \beta \right| \\ &= -\hat{E}_{1Z} \hat{E}_{2Z} + 2\hat{E}_{1Z} \hat{E}_{2Z} \hat{N}_Z - \frac{1}{2} \hat{N}_Z + \frac{\mathbf{E}}{4}\end{aligned}\quad (\text{S17})$$

from which we obtain:

$$\omega_2 \left( \hat{L}_Z^{T_0 S_0, \alpha} + \hat{L}_Z^{T_0 S_0, \beta} \right) = \omega_2 \left( \hat{E}_{1X} \hat{E}_{2X} + \hat{E}_{1Y} \hat{E}_{2Y} \right) \quad (\text{S18})$$

$$\omega_1 \left( \frac{\hat{E}^{T_0 S_0, \alpha} + \hat{E}^{T_0 S_0, \beta}}{4} \right) = \omega_1 \left( -\frac{1}{2} \hat{E}_{1Z} \hat{E}_{2Z} + \frac{\mathbf{E}}{8} \right) \quad (\text{S19})$$

The transverse fictitious  $\frac{1}{2}$ -spin operators for the proton in the  $\hat{S}_0 \hat{T}_0$  subspace are:

$$\begin{aligned}\hat{L}_X^{S_0 T_0, \alpha\beta} &= \frac{1}{2} \left( \left| \hat{S}_0^{(e1, e2)}, \alpha \right\rangle \langle \hat{T}_0^{(e1, e2)}, \beta \right| + \left| \hat{T}_0^{(e1, e2)}, \beta \right\rangle \langle \hat{S}_0^{(e1, e2)}, \alpha \right| \\ &= \frac{1}{2} \hat{E}_{1Z} \hat{N}_X - \frac{1}{2} \hat{E}_{2Z} \hat{N}_X + \hat{E}_{1X} \hat{E}_{2Y} \hat{N}_Y - \hat{E}_{1Y} \hat{E}_{2X} \hat{N}_Y\end{aligned}\quad (\text{S20})$$

$$\begin{aligned}
\hat{L}_X^{T_0 S_0, \alpha\beta} &= \frac{1}{2} \left( \left| \hat{T}_0^{(e1, e2)}, \alpha \right\rangle \left\langle \hat{S}_0^{(e1, e2)}, \beta \right| + \left| \hat{S}_0^{(e1, e2)}, \beta \right\rangle \left\langle \hat{T}_0^{(e1, e2)}, \alpha \right| \right) \\
&= \frac{1}{2} \hat{E}_{1Z} \hat{N}_X - \frac{1}{2} \hat{E}_{2Z} \hat{N}_X - \hat{E}_{1X} \hat{E}_{2Y} \hat{N}_Y + \hat{E}_{1Y} \hat{E}_{2X} \hat{N}_Y
\end{aligned} \tag{S21}$$

from which we obtain the pseudo-secular component:

$$B_\Delta \left( \hat{L}_X^{S_0 T_0, \alpha\beta} + \hat{L}_X^{T_0 S_0, \alpha\beta} \right) = B_\Delta \left( \hat{E}_{1Z} - \hat{E}_{2Z} \right) \hat{N}_X \tag{S22}$$

Longitudinal fictitious  $\frac{1}{2}$ -spin operators for the electron in the  $\hat{T}_{+1} \hat{T}_{-1}$  subspace are:

$$\begin{aligned}
\hat{L}_Z^{T_+ T_-, \alpha} &= \frac{1}{2} \left( \left| \hat{T}_{+1}^{(e1, e2)}, \alpha \right\rangle \left\langle \hat{T}_{+1}^{(e1, e2)}, \alpha \right| - \left| \hat{T}_{-1}^{(e1, e2)}, \alpha \right\rangle \left\langle \hat{T}_{-1}^{(e1, e2)}, \alpha \right| \right) \\
&= \frac{\hat{E}_{1Z}}{4} + \frac{\hat{E}_{2Z}}{4} + \frac{1}{2} \left( \hat{E}_{1Z} \hat{N}_Z \right) + \frac{1}{2} \left( \hat{E}_{2Z} \hat{N}_Z \right)
\end{aligned} \tag{S23}$$

$$\begin{aligned}
\hat{L}_Z^{T_+ T_-, \beta} &= \frac{1}{2} \left( \left| \hat{T}_{+1}^{(e1, e2)}, \beta \right\rangle \left\langle \hat{T}_{+1}^{(e1, e2)}, \beta \right| - \left| \hat{T}_{-1}^{(e1, e2)}, \beta \right\rangle \left\langle \hat{T}_{-1}^{(e1, e2)}, \beta \right| \right) \\
&= \frac{\hat{E}_{1Z}}{4} + \frac{\hat{E}_{2Z}}{4} - \frac{1}{2} \left( \hat{E}_{1Z} \hat{N}_Z \right) - \frac{1}{2} \left( \hat{E}_{2Z} \hat{N}_Z \right)
\end{aligned} \tag{S24}$$

$$\begin{aligned}
\hat{E}^{T_+ T_-, \alpha} &= \left( \left| \hat{T}_{+1}^{(e1, e2)}, \alpha \right\rangle \left\langle \hat{T}_{+1}^{(e1, e2)}, \alpha \right| + \left| \hat{T}_{-1}^{(e1, e2)}, \alpha \right\rangle \left\langle \hat{T}_{-1}^{(e1, e2)}, \alpha \right| \right) \\
&= \hat{E}_{1Z} \hat{E}_{2Z} + 2 \hat{E}_{1Z} \hat{E}_{2Z} \hat{N}_Z + \frac{\hat{N}_Z}{2} + \frac{\mathbf{E}}{4}
\end{aligned} \tag{S25}$$

$$\begin{aligned}
\hat{E}^{T_+ T_-, \beta} &= \left( \left| \hat{T}_{+1}^{(e1, e2)}, \beta \right\rangle \left\langle \hat{T}_{+1}^{(e1, e2)}, \beta \right| + \left| \hat{T}_{-1}^{(e1, e2)}, \beta \right\rangle \left\langle \hat{T}_{-1}^{(e1, e2)}, \beta \right| \right) \\
&= \hat{E}_{1Z} \hat{E}_{2Z} - 2 \hat{E}_{1Z} \hat{E}_{2Z} \hat{N}_Z - \frac{\hat{N}_Z}{2} + \frac{\mathbf{E}}{4}
\end{aligned} \tag{S26}$$

from which we obtain:

$$\omega_{\Sigma_e} \left( \hat{E}_{1Z} + \hat{E}_{2Z} \right) = 2 \omega_{\Sigma_e} \left( \hat{L}_Z^{T_+ T_-, \alpha} + \hat{L}_Z^{T_+ T_-, \beta} \right) \tag{S27}$$

$$A_\Sigma \left( \hat{E}_{1Z} \hat{N}_Z + \hat{E}_{2Z} \hat{N}_Z \right) = A_\Sigma \left( \hat{L}_Z^{T_+ T_-, \alpha} - \hat{L}_Z^{T_+ T_-, \beta} \right) \tag{S28}$$

$$\omega_1 \left( \frac{1}{2} \hat{E}_{1Z} \hat{E}_{2Z} + \frac{\mathbf{E}}{8} \right) = \omega_1 \left( \frac{\hat{E}^{T_+ T_-, \alpha} + \hat{E}^{T_+ T_-, \beta}}{4} \right) \tag{S29}$$

Finally, we introduce new transverse fictitious  $\frac{1}{2}$ -spin operators for the proton in the  $\hat{T}_{+1} \hat{T}_{-1}$  subspace given by:

$$\begin{aligned}
\hat{L}_X^{T_+ T_-, \alpha\beta} &= \frac{1}{2} \left( \left| \hat{T}_{+1}^{(e1, e2)}, \alpha \right\rangle \left\langle \hat{T}_{+1}^{(e1, e2)}, \beta \right| + \left| \hat{T}_{+1}^{(e1, e2)}, \beta \right\rangle \left\langle \hat{T}_{+1}^{(e1, e2)}, \alpha \right| \right) \\
&= \frac{1}{2} \hat{E}_{1Z} \hat{N}_X + \frac{1}{2} \hat{E}_{2Z} \hat{N}_X + \hat{E}_{1Z} \hat{E}_{2Z} \hat{N}_X + \frac{\hat{N}_X}{4}
\end{aligned} \tag{S30}$$

$$\begin{aligned}\hat{L}_X^{T_{-1},\alpha\beta} &= \frac{1}{2} \left( \left| \hat{T}_{-1}^{(e1,e2)}, \alpha \right\rangle \left\langle \hat{T}_{-1}^{(e1,e2)}, \beta \right| + \left| \hat{T}_{-1}^{(e1,e2)}, \beta \right\rangle \left\langle \hat{T}_{-1}^{(e1,e2)}, \alpha \right| \right) \\ &= -\frac{1}{2} \hat{E}_{1Z} \hat{N}_X - \frac{1}{2} \hat{E}_{2Z} \hat{N}_X + \hat{E}_{1Z} \hat{E}_{2Z} \hat{N}_X + \frac{\hat{N}_X}{4}\end{aligned}\quad (\text{S31})$$

which are needed to describe the pseudo-secular component:

$$B_\Sigma \left( \hat{L}_X^{T_{+1},\alpha\beta} - \hat{L}_X^{T_{-1},\alpha\beta} \right) = B_\Sigma \left( \hat{E}_{1Z} + \hat{E}_{2Z} \right) \hat{N}_X \quad (\text{S32})$$

The sum of these various terms, enables us to rewrite the Hamiltonian in Eq. (S8) under the action of microwave irradiation, as:

$$\hat{H}_{rot} = \hat{H}^{S_0 T_0} + \hat{H}^{T_{+1} T_{-1}} + \hat{H}_{\mu w} \quad (\text{S33})$$

where the term acting in the  $\hat{S}_0 \hat{T}_0$  space is

$$\begin{aligned}\hat{H}^{S_0 T_0} &= 2\omega_{\Delta e} \left( \hat{L}_X^{T_0 S_0, \alpha} + \hat{L}_X^{T_0 S_0, \beta} \right) + A_\Delta \left( \hat{L}_X^{T_0 S_0, \alpha} - \hat{L}_X^{T_0 S_0, \beta} \right) + B_\Delta \left( \hat{L}_X^{S_0 T_0, \alpha\beta} + \hat{L}_X^{T_0 S_0, \alpha\beta} \right) + \\ &- \omega_2 \left( \hat{L}_Z^{T_0 S_0, \alpha} + \hat{L}_Z^{T_0 S_0, \beta} \right) - \omega_1 \left( \frac{\hat{E}^{T_0 S_0, \alpha} + \hat{E}^{T_0 S_0, \beta}}{4} \right)\end{aligned}\quad (\text{S34})$$

the term acting in the  $\hat{T}_{+1} \hat{T}_{-1}$  space is:

$$\begin{aligned}\hat{H}^{T_{+1} T_{-1}} &= 2\omega_e \left( \hat{L}_Z^{T_{\pm 1}, \alpha} + \hat{L}_Z^{T_{\pm 1}, \beta} \right) \hat{R}_y^{T_{\pm 1}}(\theta) + \omega_N \hat{N}_Z + B_\Sigma \left( \hat{L}_X^{T_{+1}, \alpha\beta} - \hat{L}_X^{T_{-1}, \alpha\beta} \right) \\ &+ A_\Sigma \left( \hat{L}_Z^{T_{+1}, \alpha} - \hat{L}_Z^{T_{-1}, \beta} \right) + \omega_1 \left( \frac{\hat{E}^{T_{+1} T_{-1}, \alpha} + \hat{E}^{T_{+1} T_{-1}, \beta}}{4} \right)\end{aligned}\quad (\text{S35})$$

and  $\hat{H}_{\mu w} = \omega_{\mu w} (\hat{E}_{1X} + \hat{E}_{2X})$  is the microwave irradiation operator, with  $\omega_{\mu w}$  the strength of its nutation frequency. Here  $\omega_{\Sigma e}$  and  $\omega_{\Delta e} \sim 0$  are the sum and difference of the electron Larmor frequencies in the rotating frame,  $\hat{R}_y^{T_{\pm 1}}(\theta)$  in Eq. (S35) is a rotation matrix about the y-axis that acts on both the  $\alpha$  and  $\beta$  space; its associated  $2\omega_e \left( \hat{L}_Z^{T_{\pm 1}, \alpha} + \hat{L}_Z^{T_{\pm 1}, \beta} \right) \hat{R}_y^{T_{\pm 1}}(\theta)$  term then corresponds to  $\omega_e \cos(\theta) \left( \hat{L}_Z^{T_{\pm 1}, \alpha} + \hat{L}_Z^{T_{\pm 1}, \beta} \right) + \omega_e \sin(\theta) (\hat{E}_{1X} + \hat{E}_{2X})$ , with  $\theta = \arctan(\omega_{\mu w} / \omega_{\Sigma e})$  the angle felt by the electron's effective field, and  $\omega_e = \sqrt{\omega_{\Sigma e}^2 + \omega_{\mu w}^2}$  the effective field's strength. The matrix representation of Eq. (S33) is:

	$ \hat{S}_0^{(e1e2)}, \alpha\rangle$	$ \hat{T}_{+1}^{(e1e2)}, \alpha\rangle$	$ \hat{T}_0^{(e1e2)}, \alpha\rangle$	$ \hat{T}_{-1}^{(e1e2)}, \alpha\rangle$	$ \hat{S}_0^{(e1e2)}, \beta\rangle$	$ \hat{T}_{+1}^{(e1e2)}, \beta\rangle$	$ \hat{T}_0^{(e1e2)}, \beta\rangle$	$ \hat{T}_{-1}^{(e1e2)}, \beta\rangle$
$ \hat{S}_0^{(e1e2)}, \alpha\rangle$	$-\frac{\omega_1}{4} - \frac{\omega_2}{2} + \frac{\omega_N}{2}$	0	$\frac{A_\Delta + \omega_N}{2}$	0	0	0	$\frac{B_\Delta}{2}$	0
$ \hat{T}_{+1}^{(e1e2)}, \alpha\rangle$	0	$\frac{A_\Sigma}{2} + \frac{\omega_1}{4} + \omega_e \cos(\theta) + \frac{\omega_N}{2}$	$\frac{\omega_e \sin(\theta)}{\sqrt{2}}$	0	0	$\frac{B_\Sigma}{2}$	0	0
$ \hat{T}_0^{(e1e2)}, \alpha\rangle$	$\frac{A_\Delta + \omega_N}{2}$	$\frac{\omega_e \sin(\theta)}{\sqrt{2}}$	$-\frac{\omega_1}{4} + \frac{\omega_2}{2} + \frac{\omega_N}{2}$	$\frac{\omega_e \sin(\theta)}{\sqrt{2}}$	$\frac{B_\Delta}{2}$	0	0	0
$ \hat{T}_{-1}^{(e1e2)}, \alpha\rangle$	0	0	$\frac{\omega_e \sin(\theta)}{\sqrt{2}}$	$-\frac{A_\Sigma}{2} + \frac{\omega_1}{4} - \omega_e \cos(\theta) + \frac{\omega_N}{2}$	0	0	0	$-\frac{B_\Sigma}{2}$
$ \hat{S}_0^{(e1e2)}, \beta\rangle$	0	0	$\frac{B_\Delta}{2}$	0	$-\frac{\omega_1}{4} - \frac{\omega_2}{2} - \frac{\omega_N}{2}$	0	$-\frac{A_\Delta + \omega_N}{2}$	0
$ \hat{T}_{+1}^{(e1e2)}, \beta\rangle$	0	$\frac{B_\Sigma}{2}$	0	0	0	$-\frac{A_\Sigma}{2} + \frac{\omega_1}{4} + \omega_e \cos(\theta) - \frac{\omega_N}{2}$	$\frac{\omega_e \sin(\theta)}{\sqrt{2}}$	0
$ \hat{T}_0^{(e1e2)}, \beta\rangle$	$\frac{B_\Delta}{2}$	0	0	0	$-\frac{A_\Delta + \omega_N}{2}$	$\frac{\omega_e \sin(\theta)}{\sqrt{2}}$	$-\frac{\omega_1}{4} + \frac{\omega_2}{2} - \frac{\omega_N}{2}$	$\frac{\omega_e \sin(\theta)}{\sqrt{2}}$
$ \hat{T}_{-1}^{(e1e2)}, \beta\rangle$	0	0	0	$-\frac{B_\Sigma}{2}$	0	0	$\frac{\omega_e \sin(\theta)}{\sqrt{2}}$	$\frac{A_\Sigma}{2} + \frac{\omega_1}{4} - \omega_e \cos(\theta) - \frac{\omega_N}{2}$

(S36)

Notice that these microwave-related terms act solely within the triplet manifold mixing the  $\hat{T}_{\pm 1}^{(e1e2)}$  and  $\hat{T}_0^{(e1e2)}$  states, but do not involve the  $\hat{S}_0^{(e1e2)}$  singlet. The latter, however, is not isolated: it gets

connected to  $\hat{T}_0^{(e1e2)}$  via the difference in secular hyperfine couplings with the nucleus  $A_\Delta$ . Additional simulations –not shown– demonstrate that the pseudosecular terms are not essential for describing the J-DNP effect.

### Supporting Information 3: Defining the biradical/nuclear system population operators describing the J-DNP enhancement

The main text defines  $\hat{S}_0\hat{N}_Z$ ,  $\hat{T}_{\pm 1}\hat{N}_Z$  and  $\hat{T}_0\hat{N}_Z$  operators and relates these to the differences between the population operators  $O_\alpha$  and  $O_\beta$  (defined below), leading to the predicted nuclear polarization enhancement. As these three-spin states have to our knowledge not been previously defined, we summarize them here. To do this we rely again on Vega's two-spin triplet/single (TS) population operators,<sup>43</sup> and we direct-product them with a nuclear spin state that can be in either the  $\alpha$  or  $\beta$  state. These can be written in terms of single-spin product operators, as:

$$\begin{aligned} \hat{S}_{0,\alpha} = |\hat{S}_0^{(e1,e2)}, \alpha\rangle \langle \hat{S}_0^{(e1,e2)}, \alpha| &= \frac{\mathbf{E}}{8} + \frac{\hat{N}_Z}{4} - \frac{1}{4}(\hat{E}_{1-}\hat{E}_{2+}) - \frac{1}{4}(\hat{E}_{1+}\hat{E}_{2-}) + \\ &- \frac{1}{2}(\hat{E}_{1Z}\hat{E}_{2Z}) - \frac{1}{2}(\hat{E}_{1-}\hat{E}_{2+}\hat{N}_Z) - \frac{1}{2}(\hat{E}_{1+}\hat{E}_{2-}\hat{N}_Z) - \hat{E}_{1Z}\hat{E}_{2Z}\hat{N}_Z \end{aligned} \quad (\text{S37})$$

$$\begin{aligned} \hat{T}_{\pm 1,\alpha} = |\hat{T}_{\pm 1}^{(e1,e2)}, \alpha\rangle \langle \hat{T}_{\pm 1}^{(e1,e2)}, \alpha| &= \frac{\mathbf{E}}{8} + \frac{\hat{N}_Z}{4} + \frac{\hat{E}_{1Z}}{4} \pm \frac{\hat{E}_{2Z}}{4} + \\ &+ \frac{1}{2}(\hat{E}_{1Z}\hat{E}_{2Z}) \pm \frac{1}{2}(\hat{E}_{1Z}\hat{N}_Z) \pm \frac{1}{2}(\hat{E}_{2Z}\hat{N}_Z) + \hat{E}_{1Z}\hat{E}_{2Z}\hat{N}_Z \end{aligned} \quad (\text{S38})$$

$$\begin{aligned} \hat{T}_{0,\alpha} = |\hat{T}_0^{(e1,e2)}, \alpha\rangle \langle \hat{T}_0^{(e1,e2)}, \alpha| &= \frac{\mathbf{E}}{8} + \frac{\hat{N}_Z}{4} + \frac{1}{4}(\hat{E}_{1-}\hat{E}_{2+}) + \frac{1}{4}(\hat{E}_{1+}\hat{E}_{2-}) + \\ &- \frac{1}{2}(\hat{E}_{1Z}\hat{E}_{2Z}) + \frac{1}{2}(\hat{E}_{1-}\hat{E}_{2+}\hat{N}_Z) + \frac{1}{2}(\hat{E}_{1+}\hat{E}_{2-}\hat{N}_Z) - \hat{E}_{1Z}\hat{E}_{2Z}\hat{N}_Z \end{aligned} \quad (\text{S39})$$

$$\begin{aligned} \hat{S}_{0,\beta} = |\hat{S}_0^{(e1,e2)}, \beta\rangle \langle \hat{S}_0^{(e1,e2)}, \beta| &= \frac{\mathbf{E}}{8} - \frac{\hat{N}_Z}{4} - \frac{1}{4}(\hat{E}_{1-}\hat{E}_{2+}) - \frac{1}{4}(\hat{E}_{1+}\hat{E}_{2-}) - \\ &+ \frac{1}{2}(\hat{E}_{1Z}\hat{E}_{2Z}) + \frac{1}{2}(\hat{E}_{1-}\hat{E}_{2+}\hat{N}_Z) + \frac{1}{2}(\hat{E}_{1+}\hat{E}_{2-}\hat{N}_Z) + \hat{E}_{1Z}\hat{E}_{2Z}\hat{N}_Z \end{aligned} \quad (\text{S40})$$

$$\begin{aligned} \hat{T}_{\pm 1,\beta} = |\hat{T}_{\pm 1}^{(e1,e2)}, \beta\rangle \langle \hat{T}_{\pm 1}^{(e1,e2)}, \beta| &= \frac{\mathbf{E}}{8} - \frac{\hat{N}_Z}{4} \pm \frac{\hat{E}_{1Z}}{4} \pm \frac{\hat{E}_{2Z}}{4} + \\ &+ \frac{1}{2}(\hat{E}_{1Z}\hat{E}_{2Z}) \mp \frac{1}{2}(\hat{E}_{1Z}\hat{N}_Z) \mp \frac{1}{2}(\hat{E}_{2Z}\hat{N}_Z) - \hat{E}_{1Z}\hat{E}_{2Z}\hat{N}_Z \end{aligned} \quad (\text{S41})$$

$$\begin{aligned} \hat{T}_{0,\beta} = |\hat{T}_0^{(e1,e2)}, \beta\rangle \langle \hat{T}_0^{(e1,e2)}, \beta| &= \frac{\mathbf{E}}{8} - \frac{\hat{N}_Z}{4} + \frac{1}{4}(\hat{E}_{1-}\hat{E}_{2+}) + \frac{1}{4}(\hat{E}_{1+}\hat{E}_{2-}) - \\ &+ \frac{1}{2}(\hat{E}_{1Z}\hat{E}_{2Z}) - \frac{1}{2}(\hat{E}_{1-}\hat{E}_{2+}\hat{N}_Z) - \frac{1}{2}(\hat{E}_{1+}\hat{E}_{2-}\hat{N}_Z) + \hat{E}_{1Z}\hat{E}_{2Z}\hat{N}_Z \end{aligned} \quad (\text{S42})$$

Taking suitable differences among these states, leads to the longitudinal fictitious operators used in the main text (Figures 4-5) to describe how singlet and triplet states enhance the nuclear polarization:

$$\begin{aligned}\hat{S}_0^{(ele2)} \hat{N}_Z &= \frac{1}{2} \left( \left| \hat{S}_0^{(ele2)}, \alpha \right\rangle \langle \hat{S}_0^{(ele2)}, \alpha | - \left| \hat{S}_0^{(ele2)}, \beta \right\rangle \langle \hat{S}_0^{(ele2)}, \beta | \right) \\ &= \frac{\hat{N}_Z}{4} - \frac{1}{2} \left( \hat{E}_{1-} \hat{E}_{2+} \hat{N}_Z + \hat{E}_{1+} \hat{E}_{2-} \hat{N}_Z \right) - \hat{E}_{1Z} \hat{E}_{2Z} \hat{N}_Z\end{aligned}\quad (\text{S43})$$

$$\begin{aligned}\hat{T}_{\pm 1}^{(ele2)} \hat{N}_Z &= \frac{1}{2} \left( \left| \hat{T}_{\pm 1}^{(ele2)}, \alpha \right\rangle \langle \hat{T}_{\pm 1}^{(ele2)}, \alpha | - \left| \hat{T}_{\pm 1}^{(ele2)}, \beta \right\rangle \langle \hat{T}_{\pm 1}^{(ele2)}, \beta | \right) \\ &= \frac{\hat{N}_Z}{4} \pm \frac{1}{2} \left( \hat{E}_{1Z} \hat{N}_Z + \hat{E}_{2Z} \hat{N}_Z \right) + \hat{E}_{1Z} \hat{E}_{2Z} \hat{N}_Z\end{aligned}\quad (\text{S44})$$

$$\begin{aligned}\hat{T}_0^{(ele2)} \hat{N}_Z &= \frac{1}{2} \left( \left| \hat{T}_0^{(ele2)}, \alpha \right\rangle \langle \hat{T}_0^{(ele2)}, \alpha | - \left| \hat{T}_0^{(ele2)}, \beta \right\rangle \langle \hat{T}_0^{(ele2)}, \beta | \right) \\ &= \frac{\hat{N}_Z}{4} + \frac{1}{2} \left( \hat{E}_{1-} \hat{E}_{2+} \hat{N}_Z + \hat{E}_{1+} \hat{E}_{2-} \hat{N}_Z \right) - \hat{E}_{1Z} \hat{E}_{2Z} \hat{N}_Z\end{aligned}\quad (\text{S45})$$

#### Supporting Information 4: Additional Redfield-derived relaxation rates for the biradical/nuclear system

The main text presented a simplified version of the relaxation rates of  $\hat{S}_{0,\alpha/\beta}$ ,  $\hat{T}_{0,\alpha/\beta}$  and  $\hat{T}_{\pm 1,\alpha,\beta}$ , whose full expressions are provided here. For  $\hat{S}_{0,\alpha/\beta}$  these were:

$$\begin{aligned}-R[\hat{S}_{0,\beta}] &= \frac{\Delta_{\Delta HF}^2}{180} J(J_{\text{ex}} - \omega_E + \omega_N) + \frac{\Delta_{\Delta HF}^2}{30} J(J_{\text{ex}} + \omega_E + \omega_N) + \frac{\Delta_{\text{CSA}}^2}{15} J(\omega_N) + \frac{\Delta_{\Delta HF}^2}{60} J(J_{\text{ex}} + \omega_N) + \\ &+ \frac{[\Delta_{\Delta HF}^2 + 4\aleph_{\Delta G, \Delta G - \Delta HF}]}{90} J(J_{\text{ex}}) + \frac{[\Delta_{\Delta HF}^2 + 4\aleph_{\Delta G, \Delta G - \Delta HF}]}{120} J(J_{\text{ex}} - \omega_E) + \frac{[\Delta_{\Delta HF}^2 + 4\aleph_{\Delta G, \Delta G - \Delta HF}]}{120} J(J_{\text{ex}} + \omega_E)\end{aligned}\quad (\text{S46})$$

and

$$\begin{aligned}-R[\hat{S}_{0,\alpha}] &= \frac{\Delta_{\Delta HF}^2}{180} J(J_{\text{ex}} + \omega_E - \omega_N) + \frac{\Delta_{\Delta HF}^2}{30} J(J_{\text{ex}} - \omega_E - \omega_N) + \frac{\Delta_{\text{CSA}}^2}{15} J(\omega_N) + \frac{\Delta_{\Delta HF}^2}{60} J(J_{\text{ex}} - \omega_N) + \\ &+ \frac{[\Delta_{\Delta HF}^2 + 4\aleph_{\Delta G, \Delta G + \Delta HF}]}{90} J(J_{\text{ex}}) + \frac{[\Delta_{\Delta HF}^2 + 4\aleph_{\Delta G, \Delta G + \Delta HF}]}{120} J(J_{\text{ex}} - \omega_E) + \frac{[\Delta_{\Delta HF}^2 + 4\aleph_{\Delta G, \Delta G + \Delta HF}]}{120} J(J_{\text{ex}} + \omega_E)\end{aligned}\quad (\text{S47})$$

For the  $\hat{T}_{\pm 1,\alpha/\beta}$  states these were:

$$\begin{aligned}-R[\hat{T}_{+1,\beta}] &= \frac{\Delta_{\Delta HF}^2}{180} J(J_{\text{ex}} + \omega_E - \omega_N) + \frac{[\Delta_{\Delta HF}^2 + 4\aleph_{\Delta G, \Delta G - \Delta HF}]}{120} J(J_{\text{ex}} + \omega_E) + \\ &+ \frac{[\Delta_{\Sigma HF}^2 + 4\aleph_{\text{CSA}, \text{CSA} + \Sigma HF}]}{60} J(\omega_N) + \frac{[5\Delta_{\Sigma HF}^2 + 12\aleph_{\text{EE} + \Sigma G, (\text{EE} + \Sigma G) - \Sigma HF}]}{360} J(\omega_E) + \frac{\Delta_{\text{EE}}^2}{15} J(2\omega_E)\end{aligned}\quad (\text{S48})$$

and

$$\begin{aligned}-R[\hat{T}_{+1,\alpha}] &= \frac{\Delta_{\Delta HF}^2}{30} J(J_{\text{ex}} + \omega_E + \omega_N) + \frac{[\Delta_{\Delta HF}^2 + 4\aleph_{\Delta G, \Delta G + \Delta HF}]}{120} J(J_{\text{ex}} + \omega_E) + \\ &+ \frac{[\Delta_{\Sigma HF}^2 + 4\aleph_{\text{CSA}, \text{CSA} + \Sigma HF}]}{60} J(\omega_N) + \frac{[5\Delta_{\Sigma HF}^2 + 4\aleph_{\text{EE} + \Sigma G, (\text{EE} + \Sigma G) + \Sigma HF}]}{120} J(\omega_E) + \frac{\Delta_{\text{EE}}^2}{15} J(2\omega_E)\end{aligned}\quad (\text{S49})$$

For the  $\hat{T}_{0,\alpha/\beta}$ , the self-relaxation rates are

$$\begin{aligned}-R[\hat{T}_{0,\beta}] &= \frac{\Delta_{\text{CSA}}^2}{15} J(\omega_N) + \frac{\Delta_{\Delta HF}^2}{60} J(J_{\text{ex}} - \omega_N) + \\ &+ \frac{[\Delta_{\Delta HF}^2 + 4\aleph_{\Delta G, \Delta G - \Delta HF}]}{90} J(J_{\text{ex}}) + \frac{[6\Delta_{\text{EE}}^2 + 5\Delta_{\Sigma HF}^2 + 6\aleph_{\Sigma G, \Sigma G - \Sigma HF}]}{90} J(\omega_E)\end{aligned}\quad (\text{S50})$$

and

$$\begin{aligned}
-R[\hat{T}_{0,\alpha}] &= \frac{\Delta_{\text{CSA}}^2}{15} J(\omega_{\text{N}}) + \frac{\Delta_{\text{AHF}}^2}{60} J(J_{\text{ex}} + \omega_{\text{N}}) + \\
&+ \frac{[\Delta_{\text{AHF}}^2 + 4\aleph_{\Delta\text{G},\Delta\text{G}+\Delta\text{HF}}]}{90} J(J_{\text{ex}}) + \frac{[6\Delta_{\text{EE}}^2 + 5\Delta_{\Sigma\text{HF}}^2 + 6\aleph_{\Sigma\text{G},\Sigma\text{G}+\Sigma\text{HF}}]}{90} J(\omega_{\text{E}})
\end{aligned} \tag{S51}$$

And for  $\hat{T}_{-1,\alpha/\beta}$  the self-relaxation rates were:

$$\begin{aligned}
-R[\hat{T}_{-1,\beta}] &= \frac{\Delta_{\text{AHF}}^2}{30} J(J_{\text{ex}} - \omega_{\text{E}} - \omega_{\text{N}}) + \frac{[\Delta_{\text{AHF}}^2 + 4\aleph_{\Delta\text{G},\Delta\text{G}-\Delta\text{HF}}]}{120} J(J_{\text{ex}} - \omega_{\text{E}}) + \\
&+ \frac{[\Delta_{\Sigma\text{HF}}^2 + 4\aleph_{\text{CSA},\text{CSA}-\Sigma\text{HF}}]}{60} J(\omega_{\text{N}}) + \frac{[5\Delta_{\Sigma\text{HF}}^2 + 4\aleph_{\text{EE}-\Sigma\text{G},\text{EE}-\Sigma\text{G}+\Sigma\text{HF}}]}{120} J(\omega_{\text{E}}) + \frac{\Delta_{\text{EE}}^2}{15} J(2\omega_{\text{E}})
\end{aligned} \tag{S52}$$

and

$$\begin{aligned}
-R[\hat{T}_{-1,\alpha}] &= \frac{\Delta_{\text{AHF}}^2}{180} J(J_{\text{ex}} - \omega_{\text{E}} + \omega_{\text{N}}) + \frac{[\Delta_{\text{AHF}}^2 + 4\aleph_{\Delta\text{G},\Delta\text{G}+\Delta\text{HF}}]}{120} J(J_{\text{ex}} - \omega_{\text{E}}) + \\
&+ \frac{[\Delta_{\Sigma\text{HF}}^2 + 4\aleph_{\text{CSA},\text{CSA}-\Sigma\text{HF}}]}{60} J(\omega_{\text{N}}) + \frac{[5\Delta_{\Sigma\text{HF}}^2 + 12\aleph_{\text{EE}-\Sigma\text{G},\text{EE}-\Sigma\text{G}-\Sigma\text{HF}}]}{360} J(\omega_{\text{E}}) + \frac{\Delta_{\text{EE}}^2}{15} J(2\omega_{\text{E}})
\end{aligned} \tag{S53}$$

These expressions were all derived taking the possibility of having the spins' relaxation driven by the nuclear chemical shift anisotropy tensor (**CSA**), by  $\Delta\mathbf{G} = \mathbf{G}_1 - \mathbf{G}_2$  and by  $\Delta\mathbf{HF} = \mathbf{HFC}_1 - \mathbf{HFC}_2$  anisotropies deriving from tensors associated to the differences between the two  $g$ - and electron/nuclear hyperfine coupling tensors, respectively; by tensors  $\Sigma\mathbf{G} = \mathbf{G}_1 + \mathbf{G}_2$  and  $\Sigma\mathbf{HF} = \mathbf{HFC}_1 + \mathbf{HFC}_2$  associated to the sums of these two electron  $g$ - and hyperfine tensors, and by the **EE** interaction representing the dipolar tensor between the two. As is usual in spin relaxation theory<sup>22,23</sup>, all these rates contain combinations of second-rank norms squared  $\Delta_{\mathbf{A}}^2$  of all the aforementioned tensors **A**, second-rank scalar products  $\aleph_{\mathbf{A},\mathbf{B}}$  of 3x3 tensors **A** and **B**<sup>42</sup>, and linear combinations of these products among various tensors, as given in Supporting Information 5. Figures S4 and S5 below expand this matter further, by showing how rates of the  $\alpha$  and  $\beta$  nuclear sub-states of  $\hat{S}_0$ ,  $\hat{T}_0$  and  $\hat{T}_{\pm 1}$  vary, when  $J_{\text{ex}}$  matches  $\pm(\omega_{\text{E}} + \omega_{\text{N}})$  – this time as a function of  $B_0$  and  $\tau_{\text{c}}$ .

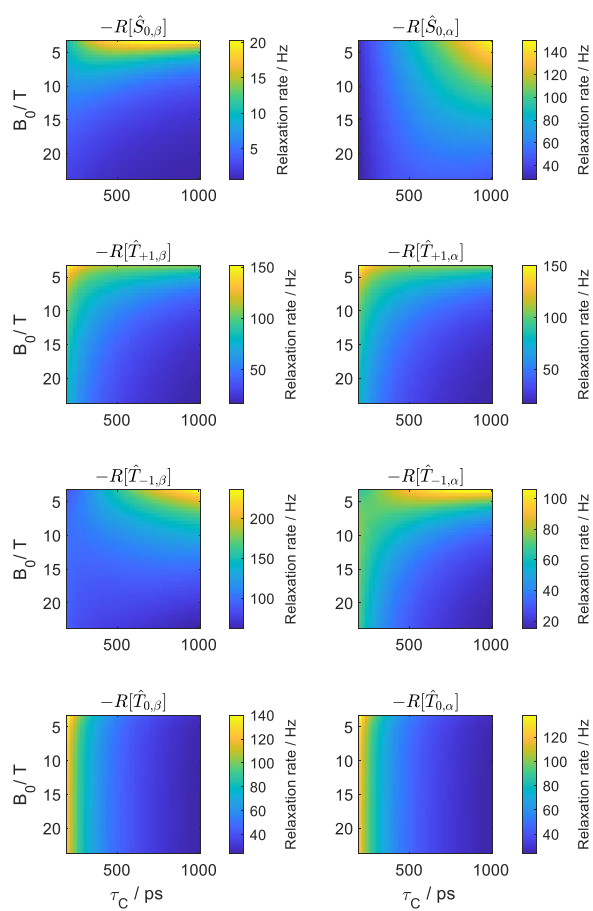


**Fig. S4:** Numerically calculated self-relaxation rates of  $\hat{S}_{0,\alpha/\beta}$ ,  $\hat{T}_{0,\alpha/\beta}$  and  $\hat{T}_{\pm 1,\alpha/\beta}$  as a function of  $B_0$  and of the  $\tau_C$  of the biradical/proton triad, when  $J_{\text{ex}}$  is positive and equal to  $J_{\text{ex}} = -(\omega_E + \omega_N)$ . Other simulation parameters are given in Table 1.

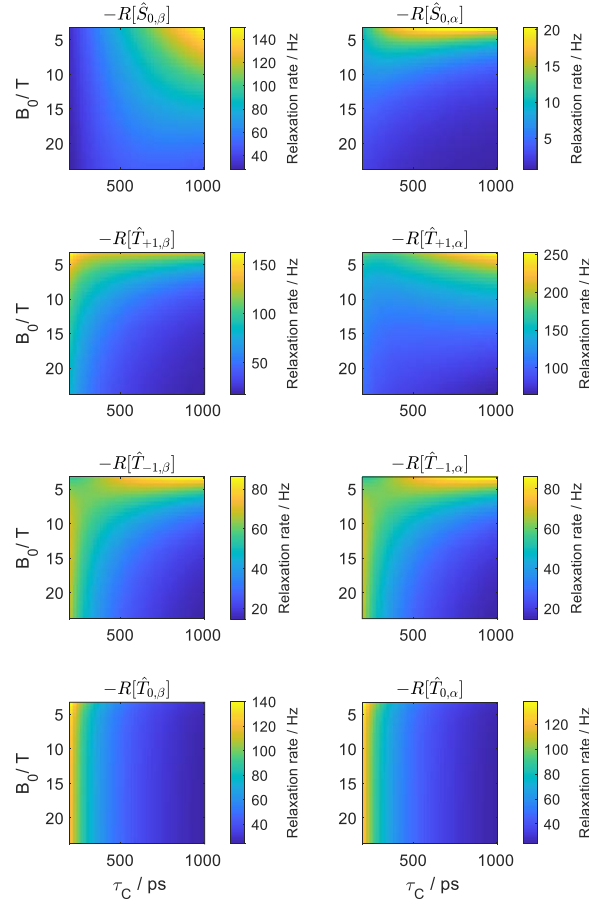


**Fig. S5:** Numerically calculated self-relaxation rates of  $\hat{S}_{0,\alpha/\beta}$ ,  $\hat{T}_{0,\alpha/\beta}$  and  $\hat{T}_{\pm 1,\alpha/\beta}$  as a function of  $B_0$  and of the  $\tau_C$  of the biradical/proton triad, when  $J_{\text{ex}}$  is negative and equal to  $J_{\text{ex}} = +(\omega_E + \omega_N)$ . Other simulation parameters are given in Table 1.

Notice how these rates decrease with magnetic field and change differentially for  $\alpha/\beta$  states with the correlation time. The main text presented how the rates of  $\hat{S}_{0,\alpha/\beta}$ ,  $\hat{T}_{0,\alpha/\beta}$  and  $\hat{T}_{\pm 1,\alpha/\beta}$  changed with exchange coupling and magnetic field, according to numerical and analytical predictions. For completion this section derives the expressions predicted by this theory, for the  $\hat{N}_Z\hat{T}_{\pm 1}$ ,  $\hat{N}_Z\hat{T}_0$  and  $\hat{S}_0\hat{N}_Z$  states.

$$\begin{aligned}
-R[\hat{N}_Z\hat{S}_0] &= \frac{2\Delta_{\text{CSA}}^2}{15} J(\omega_N) + \frac{\Delta_{\text{AHF}}^2}{120} [J(J_{\text{ex}} - \omega_N) + J(J_{\text{ex}} + \omega_N)] + \\
&+ \frac{\Delta_{\text{AHF}}^2}{60} [J(J_{\text{ex}} - \omega_E - \omega_N) + J(J_{\text{ex}} + \omega_E + \omega_N)] + \\
&+ \frac{\Delta_{\text{AHF}}^2}{360} [J(J_{\text{ex}} + \omega_E - \omega_N) + J(J_{\text{ex}} - \omega_E + \omega_N)] + \\
&+ \frac{\Delta_{\text{AHF}}^2 + 4\Delta_{\text{AG}}^2}{90} J(J_{\text{ex}}) + \frac{\Delta_{\text{AHF}}^2 + 4\Delta_{\text{AG}}^2}{120} [J(J_{\text{ex}} - \omega_E) + J(J_{\text{ex}} + \omega_E)]
\end{aligned} \tag{S54}$$

$$\begin{aligned}
-R[\hat{N}_Z\hat{T}_{+1}] &= \frac{\Delta_{\text{EE}}^2}{15} J(2\omega_E) + \frac{\Delta_{\text{AHF}}^2}{360} J(J_{\text{ex}} + \omega_E - \omega_N) + \frac{\Delta_{\text{AHF}}^2}{60} J(J_{\text{ex}} + \omega_E + \omega_N) + \\
&\frac{\Delta_{\text{AHF}}^2 + 4\Delta_{\text{AG}}^2}{120} J(J_{\text{ex}} + \omega_E) + \frac{[\Delta_{\text{AHF}}^2 + 4\Delta_{\text{CSA,CSA}+\Sigma\text{HF}}]}{30} J(\omega_N) + \frac{[5\Delta_{\text{AHF}}^2 + 6\Delta_{\text{EE}+\Sigma\text{G}}]}{180} J(\omega_E)
\end{aligned} \tag{S55}$$

$$\begin{aligned}
-R[\hat{N}_Z\hat{T}_{-1}] &= \frac{\Delta_{EE}^2}{15} J(2\omega_E) + \frac{\Delta_{AHF}^2}{360} J(J_{ex} - \omega_E + \omega_N) + \frac{\Delta_{AHF}^2}{60} J(J_{ex} - \omega_E - \omega_N) + \\
&\frac{\Delta_{AHF}^2 + 4\Delta_{AG}^2}{120} J(J_{ex} - \omega_E) + \frac{[\Delta_{\Sigma HF}^2 + 4\Delta_{CSA, CSA-\Sigma HF}^2]}{30} J(\omega_N) + \frac{[5\Delta_{\Sigma HF}^2 + 6\Delta_{EE-\Sigma G}^2]}{180} J(\omega_E)
\end{aligned} \tag{S56}$$

$$\begin{aligned}
-R[\hat{N}_Z\hat{T}_0] &= \frac{2\Delta_{CSA}^2}{15} J(\omega_N) + \frac{\Delta_{AHF}^2}{120} [J(J_{ex} - \omega_N) + J(J_{ex} + \omega_N)] + \\
&+ \frac{\Delta_{AHF}^2 + 4\Delta_{AG}^2}{90} J(J_{ex}) + \frac{[6\Delta_{EE}^2 + 5\Delta_{\Sigma HF}^2 + 6\Delta_{\Sigma G}^2]}{90} J(\omega_E)
\end{aligned} \tag{S57}$$

where the meaning of the various constants and functions are the same as in Eqs. (S46) - (S53). Figures S6 and S7 present how these rates depend on the magnetic fields and on the rotational correlation times.

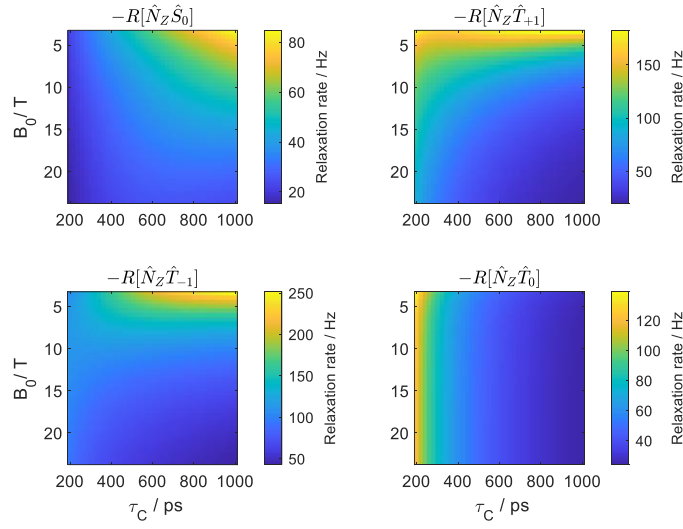


**Fig. S6:** Self-relaxation rates of  $\hat{N}_Z\hat{S}_0$ ,  $\hat{N}_Z\hat{T}_{\pm 1}$  and  $\hat{N}_Z\hat{T}_0$  states calculated as a function of  $B_0$  and of the  $\tau_C$  of the biradical/proton triad, for  $J_{ex} = -(\omega_E + \omega_N)$ . Other simulation parameters are given in Table 1.

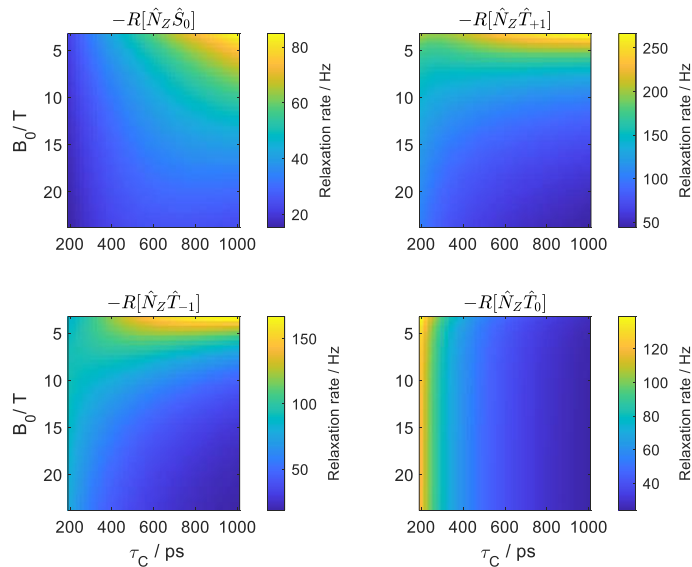


**Fig. S7:** Self-relaxation rates of  $\hat{N}_Z\hat{S}_0$ ,  $\hat{N}_Z\hat{T}_{\pm 1}$  and  $\hat{N}_Z\hat{T}_0$  states calculated as a function of  $B_0$  and of the  $\tau_C$  of the biradical/proton triad, at  $J_{ex} = +(\omega_E + \omega_N)$ . Other simulation parameters are given in Table 1.

### Supporting Information 5: Additional information about the Redfield analysis of the biradical/nuclear system

The rate expressions derived by the Redfield theory analysis for the three-spin system in Eqs. (5)-(12) of the main text, and in Eqs. S1 - S6 and S46 -S57 in the Supporting Information, were expressed on the basis of the second-rank square norms and scalar products of 3x3 tensors:

$$\begin{aligned} \aleph_{\mathbf{A},\mathbf{B}} &= \frac{\Delta_{\mathbf{A}+\mathbf{B}}^2 - \Delta_{\mathbf{A}-\mathbf{B}}^2}{4} \\ \Delta_{\mathbf{A}}^2 &= a_{XX}^2 + a_{YY}^2 + a_{ZZ}^2 - a_{XX}a_{YY} - a_{XX}a_{ZZ} - a_{YY}a_{ZZ} + \\ &+ \frac{3}{4} \left[ (a_{XY} + a_{YX})^2 + (a_{XZ} + a_{ZX})^2 + (a_{YZ} + a_{ZY})^2 \right] \end{aligned} \quad (\text{S58})$$

where  $\Delta_{\mathbf{A}}$  is the second-rank norm squared of a tensor  $\mathbf{A}$  and  $\aleph_{\mathbf{A},\mathbf{B}}$  is the second-rank scalar product between two 3x3 interaction tensors  $\mathbf{A}$  and  $\mathbf{B}$ . They can also contain linear combinations of more than two tensors and are often expressed based on the following algebraic relation:

$$\begin{aligned} \Delta_{\mathbf{A}-\mathbf{B}}^2 &= \Delta_{\mathbf{A}}^2 + \Delta_{\mathbf{B}}^2 - 2\aleph_{\mathbf{A},\mathbf{B}}, \quad \Delta_{\mathbf{A}+\mathbf{B}}^2 = \Delta_{\mathbf{A}}^2 + \Delta_{\mathbf{B}}^2 + 2\aleph_{\mathbf{A},\mathbf{B}}, \\ \Delta_{\mathbf{A}+(\mathbf{B}+\mathbf{C})}^2 &= \Delta_{\mathbf{A}}^2 + \Delta_{\mathbf{B}+\mathbf{C}}^2 + 2\aleph_{\mathbf{A},\mathbf{B}+\mathbf{C}}, \quad \Delta_{\mathbf{A}-(\mathbf{B}+\mathbf{C})}^2 = \Delta_{\mathbf{A}}^2 + \Delta_{\mathbf{B}+\mathbf{C}}^2 - 2\aleph_{\mathbf{A},\mathbf{B}+\mathbf{C}}, \\ \Delta_{\mathbf{A}-\mathbf{B}}^2 &= \aleph_{\mathbf{A}-\mathbf{B},\mathbf{A}-\mathbf{B}}, \quad \Delta_{\mathbf{A}+\mathbf{B}}^2 = \aleph_{\mathbf{A}+\mathbf{B},\mathbf{A}+\mathbf{B}}, \\ \aleph_{\mathbf{A},\mathbf{B}+\mathbf{C}} &= \aleph_{\mathbf{A},\mathbf{B}} + \aleph_{\mathbf{A},\mathbf{C}}, \quad \aleph_{\mathbf{A},\mathbf{B}-\mathbf{C}} = \aleph_{\mathbf{A},\mathbf{B}} - \aleph_{\mathbf{A},\mathbf{C}}, \\ \aleph_{\mathbf{A}+(\mathbf{D}+\mathbf{E}),\mathbf{B}+\mathbf{C}} &= \aleph_{\mathbf{A},\mathbf{B}+\mathbf{C}} + \aleph_{\mathbf{D}+\mathbf{E},\mathbf{B}+\mathbf{C}}, \\ \aleph_{\mathbf{A}-\mathbf{D},\mathbf{B}+\mathbf{C}} &= \aleph_{\mathbf{A},\mathbf{B}+\mathbf{C}} + \aleph_{-\mathbf{D},\mathbf{B}+\mathbf{C}} \\ \aleph_{\mathbf{A}-\mathbf{B},-(\mathbf{C}-\mathbf{D})} + \aleph_{\mathbf{A}-\mathbf{B},\mathbf{A}-\mathbf{B}} &= \aleph_{\mathbf{A}-\mathbf{B},(\mathbf{A}-\mathbf{B})-(\mathbf{C}-\mathbf{D})}, \quad \aleph_{\mathbf{A}+\mathbf{B},-(\mathbf{C}+\mathbf{D})} + \aleph_{\mathbf{A}+\mathbf{B},\mathbf{A}+\mathbf{B}} = \aleph_{\mathbf{A}+\mathbf{B},(\mathbf{A}+\mathbf{B})-(\mathbf{C}+\mathbf{D})} \\ \aleph_{\mathbf{A}-\mathbf{B},\mathbf{C}-\mathbf{D}} + \aleph_{\mathbf{A}-\mathbf{B},\mathbf{A}-\mathbf{B}} &= \aleph_{\mathbf{A}-\mathbf{B},(\mathbf{A}-\mathbf{B})+(\mathbf{C}-\mathbf{D})}, \quad \aleph_{\mathbf{A}+\mathbf{B},\mathbf{C}+\mathbf{D}} + \aleph_{\mathbf{A}+\mathbf{B},\mathbf{A}+\mathbf{B}} = \aleph_{\mathbf{A}+\mathbf{B},(\mathbf{A}+\mathbf{B})+(\mathbf{C}+\mathbf{D})} \end{aligned} \quad (\text{S59})$$

## Supporting Information 6: J-DNP enhancements for other kinds of biradical/nuclear systems

Table 1 in the main text focused on one combination of electron and nuclear spin coupling parameters, leading to the features noted in the paper. The two electrons had identical  $g$ -tensors, with electron and nuclear Zeeman couplings made anisotropic for the sake of realism. This section summarized three additional sets of combinations, as per the parameters summarized in Table S3. These include (i) the same coupling parameters as in Table 1 but for a different placement of the nucleus, which was now assumed devoid of chemical shift anisotropy; (ii) same parameters as in Table 1 but now with electron sites endowed with identical rhombic  $g$ -tensors; (iii) same parameters as in Table 1 but now with the electrons devoid of  $g$ -anisotropies; (iv) same parameters as in Table 1 but now with electron sites endowed with different isotropic  $g$ -tensors. The systems in the Table S3 thus contain axial, rhombic and isotropic  $g$ -tensors –in the latter case with coinciding and non-coinciding isotropic values. For the sake of conciseness, only the time-domain J-DNP transient enhancements were calculated for these scenarios –using the single optimal  $J_{ex} = +(\omega_E + \omega_N)$  but as function of  $B_0$  and  $\tau_c$ . These are shown in Figures S8-S11. Note how similar is the behaviour for all these systems, when compared with that shown in Figure 3.

**Table S3:** Biradical / proton magnetic resonance parameters used in the simulations shown in Figures S8-S11. Each electron in the biradical had its parameters modelled on a trityl center, and the nucleus was placed along the linker closer to one of the electrons.  $B_0$ ,  $J_{ex}$  and  $\tau_c$  for the biradical/proton triad were set as described in the figures; all other hyperfine coupling parameters relied on the distances.

Parameter	System i	System ii	System iii	System iv
$^1\text{H}$ chemical shift tensor, ppm	[10 10 10]	[5 10 20]	[5 10 20]	[5 10 20]
$g$ -tensor <sup>1</sup> for the electron 1 and 2, Bohr magneton	[2.0032 2.0032 2.0026]	[2.0030 2.0025 2.0020]	[2.0032 2.0032 2.0032]	$g_1$ =[2.0032 2.0032 2.0032] $g_2$ =[2.0027 2.0027 2.0027]
$^1\text{H}$ coordinates, [x y z], Å	[-3 0.5 1.3]	[-3 0.5 1.3]	[-3 0.5 1.3]	[-3 0.5 1.3]
Electron 1 coordinates, [x y z], Å	[0 0 -9.37]	[0 0 -9.37]	[0 0 -9.37]	[0 0 -9.37]
Electron 2 coordinates, [x y z], Å	[0 0 9.37]	[0 0 9.37]	[0 0 9.37]	[0 0 9.37]
Scalar relaxation modulation depth /GHz	3	3	3	1
Scalar relaxation modulation time, ps	1	1	1	1
Temperature/ K	298	298	298	298

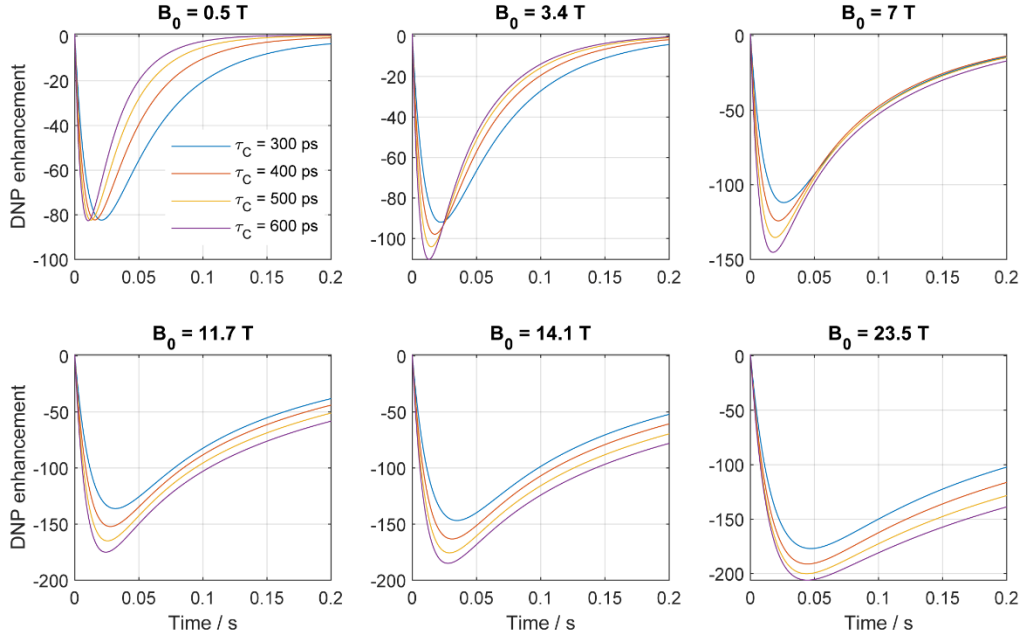


**Fig. S8:** Time domain simulations showing the evolution of the transient J-DNP enhancement as a function of  $B_0$  and of  $\tau_C$ . For all fields  $J_{ex}$  was tuned to  $+(\omega_E + \omega_N)$ , using the parameters of the system (i) in Table S3.

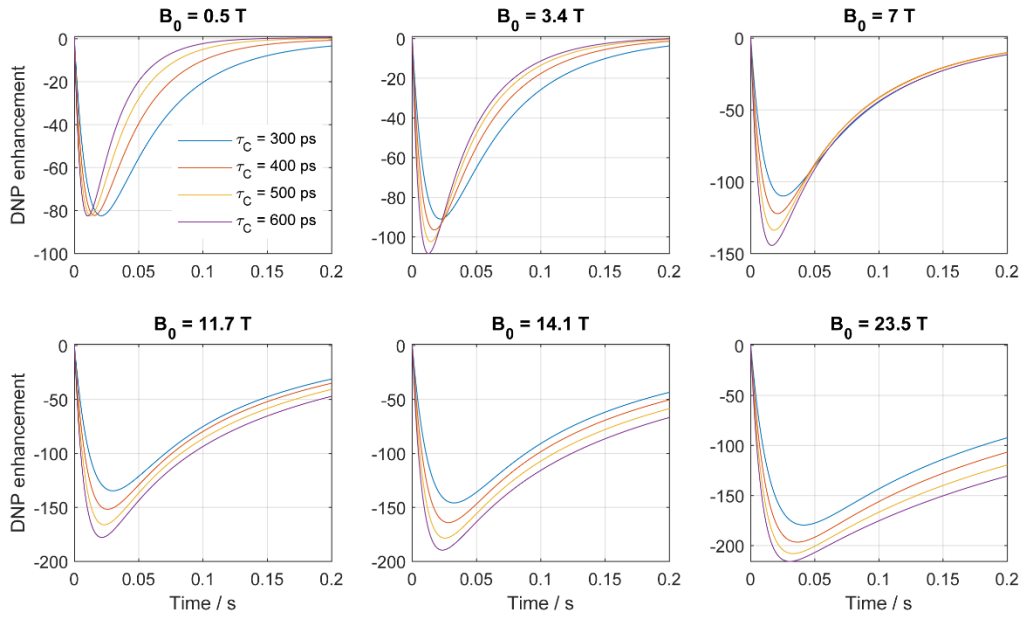


**Fig. S9:** Time domain simulations showing the evolution of the transient J-DNP enhancement as a function of  $B_0$  and of  $\tau_C$ . For all fields  $J_{ex}$  was tuned to  $+(\omega_E + \omega_N)$ , using the parameters of the system (ii) in Table S3.

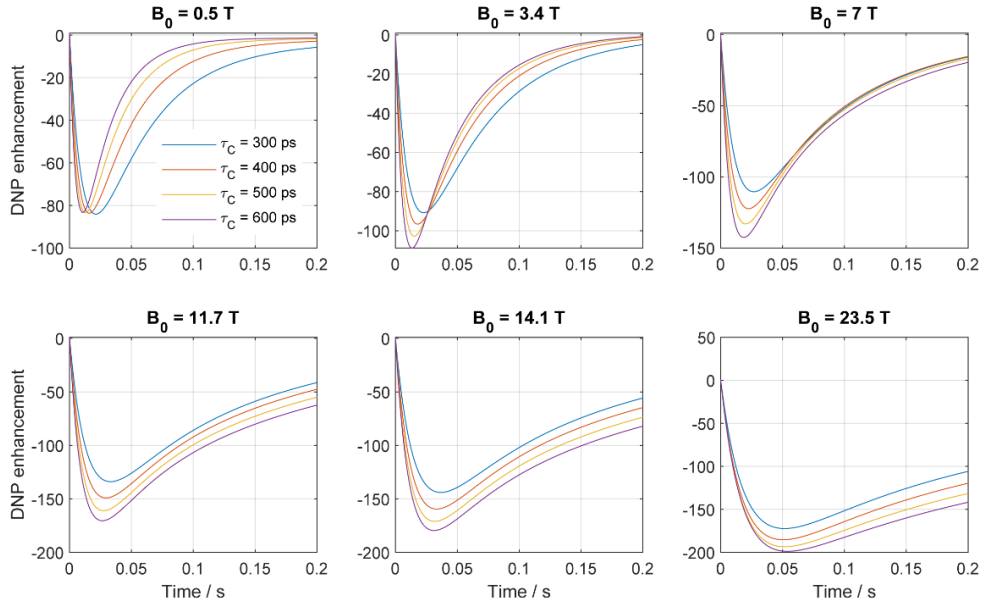


**Fig. S10:** Time domain simulations showing the evolution of the transient J-DNP enhancement as a function of  $B_0$  and of  $\tau_C$ . For all fields  $J_{ex}$  was tuned to  $+(\omega_E + \omega_N)$ , using the parameters of the system (iii) in Table S3.

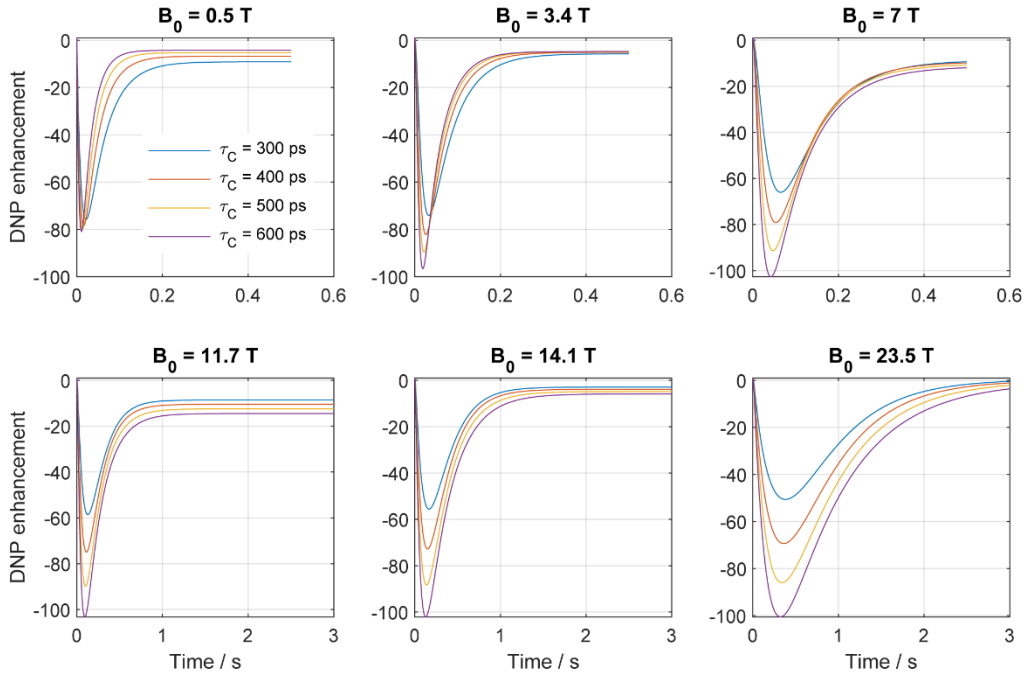


**Fig. S11:** Time domain simulations showing the evolution of the transient J-DNP enhancement as a function of  $B_0$  and of  $\tau_C$ . For all fields  $J_{ex}$  was tuned to  $+(\omega_E + \omega_N)$ , using the parameters of the system (iv) in Table S3.

Despite the noted similarity among all these cases, it is important to remark that cases will also arise where the J-DNP enhancement will be “killed”, Figures S12 - S14 include three of such instances. In the first of these, the nucleus is symmetrically placed in-between two identical electrons, that would otherwise lead to enhancement; this makes the differential “CIDNP-like” effect stop working. J-DNP requires differential hyperfine couplings driving a differential relaxation-based “nuclear spin-state filter”, in their absence, for instance if the nucleus is symmetrically placed between the two electrons (Supporting Figure S12), no enhancement results. The second case involves two electron sites endowed with different anisotropic  $g$ -tensors (Supporting Figure S13); in such instance the  $\kappa_{\Delta G, \Delta G \pm \Delta HF}$

terms overtake the  $\Delta_{\text{HFC}}^2$  in Eqs. (5) – (12), robbing J-DNP for its efficiency even when  $J_{\text{ex}} = \pm(\omega_{\text{E}} + \omega_{\text{N}})$ . Notice that this does not happen when  $g_{1,\text{iso}} = g_{2,\text{iso}}$  (Supporting Figure S11), as the  $\aleph_{\Delta\text{G},\Delta\text{G}\pm\Delta\text{HF}}$  terms still remain then smaller than  $\Delta_{\text{HFC}}^2$ . Finally, the enhancement will tend to zero if the nucleus remains too distant from the biradical: for instance, a proton placed 20 Å away from the biradical that may require over 1 s to achieve significant polarization gains, a time by which the DNP effect will lose against competing pathways. Interestingly, despite J-DNP's origin in effects related to second-rank spherical anisotropies, its nuclear enhancement never changes sign (Supporting Figure S14).

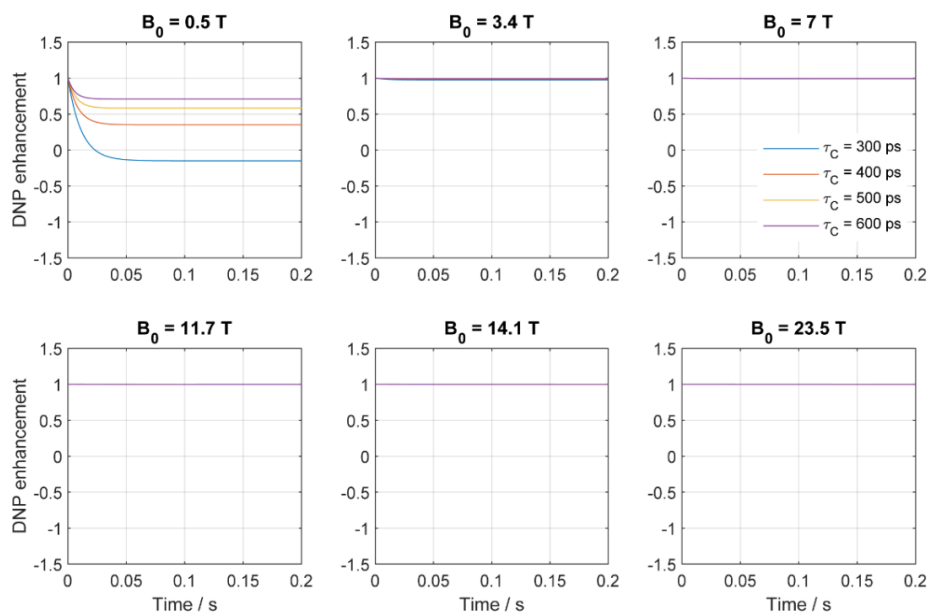


**Fig. S12:** Time domain simulations showing the evolution of the transient J-DNP enhancement as a function of  $B_0$  and of  $\tau_C$ . For all fields  $J_{\text{ex}}$  was tuned to  $+(\omega_{\text{E}} + \omega_{\text{N}})$ , using the parameters of the system in Table 1, but with the proton placed symmetrically in the biradical's centre (i.e, at [0 0 0] Å).

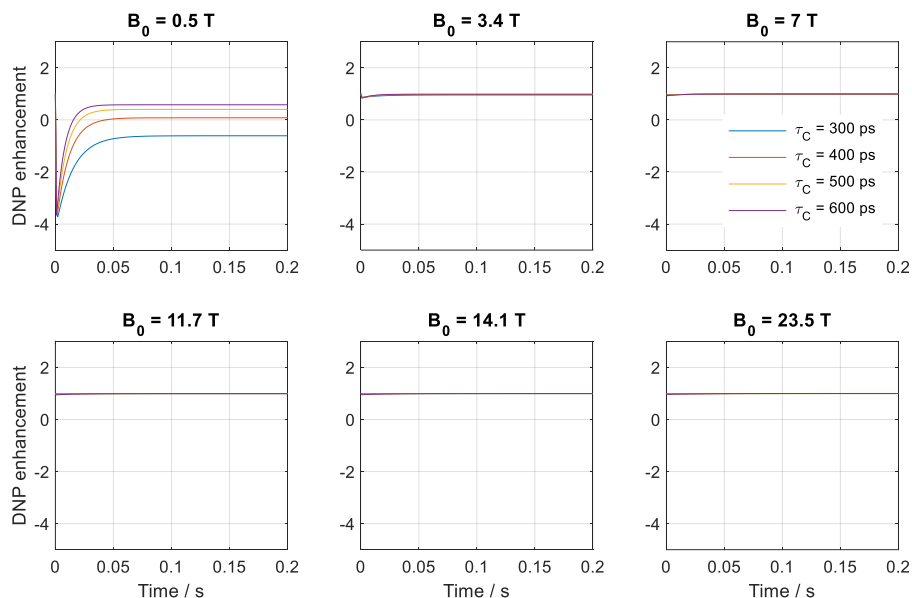


**Fig. S12:** Time domain simulations showing the evolution of the transient J-DNP enhancement as a function of  $B_0$  and of  $\tau_C$ . For all fields  $J_{\text{ex}}$  was tuned to  $+(\omega_{\text{E}} + \omega_{\text{N}})$ , using the same parameters as in Table 1 but now with electron sites endowed with different anisotropic  $g$ -tensors equal to:  $g_1=[2.0032 \ 2.0032 \ 2.0026]$  and  $g_2=[2.0032 \ 2.0032 \ 2.0023]$ .

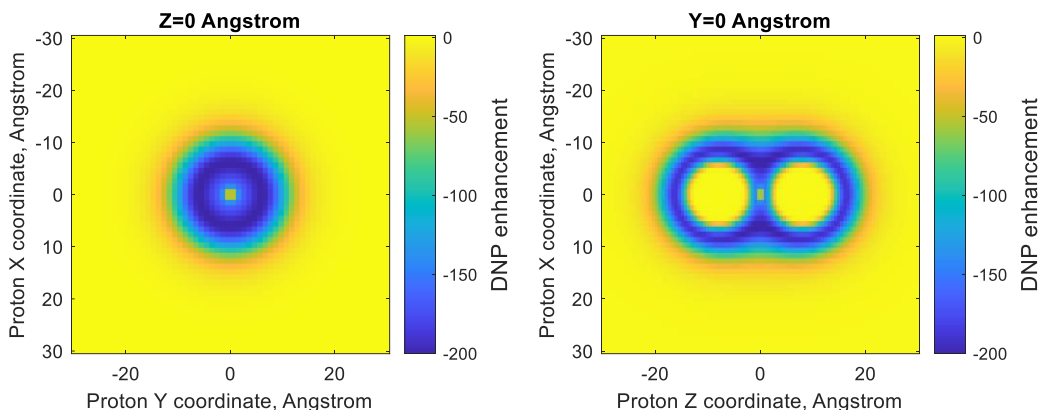


**Fig. S14:** Maximum enhancement (amplitude of  $\hat{N}_Z$  normalized to the thermal equilibrium value of a single proton at the same magnetic field) achieved within 20 ms of microwave irradiation at the electron Larmor frequency, as a function of random  $^1\text{H}$ -coordinates surrounding a model biradical. Parameters included  $B_0 = 14.08$  T,  $\tau_c = 500$  ps of the biradical/proton triad, other conditions as given in Table 1. Notice the negative enhancement displayed by all positions surrounding the radical. This is important, as otherwise the spatial averaging brought about by molecular translations, could end up being smaller or even zero.

## References

- 1 Owenius, R., Eaton, G. R. & Eaton, S. S. Frequency (250 MHz to 9.2 GHz) and viscosity dependence of electron spin relaxation of triarylmethyl radicals at room temperature. *Journal of Magnetic Resonance* **172**, 168, (2005).
- 2 Yong, L. *et al.* Electron spin relaxation of triarylmethyl radicals in fluid solution. *J Magn Reson* **152**, 156, (2001).
- 3 Blicharski, J. Nuclear magnetic relaxation by anisotropy of the chemical shift. *Z Naturforsch Pt A* **27**, 1456 (1972).
- 4 Kuprov, I., Wagner-Rundell, N. & Hore, P. Bloch-Redfield-Wangsness theory engine implementation using symbolic processing software. *Journal of Magnetic Resonance* **184**, 196 (2007).
- 5 Ardenkjaer-Larsen, J. H. *et al.* EPR and DNP properties of certain novel single electron contrast agents intended for oximetric imaging. *Journal of Magnetic Resonance* **133**, 1, doi:DOI 10.1006/jmre.1998.1438 (1998).
- 6 Hausser, K. H. & Stehlik, D. in *Advances in Magnetic and Optical Resonance* Vol. 3 79 (Elsevier, 1968).
- 7 Griesinger, C. *et al.* Dynamic nuclear polarization at high magnetic fields in liquids. *Progress in Nuclear Magnetic Resonance Spectroscopy* **64**, 4, (2012).
- 8 Prisner, T., Denysenkov, V. & Sezer, D. Liquid state DNP at high magnetic fields: Instrumentation, experimental results and atomistic modelling by molecular dynamics simulations. *Journal of Magnetic Resonance* **264**, 68, (2016).
- 9 Parigi, G., Ravera, E., Bennati, M. & Luchinat, C. Understanding Overhauser Dynamic Nuclear Polarisation through NMR relaxometry. *Mol Phys* **117**, 888, (2019).
- 10 Levien, M., Hiller, M., Tkach, I., Bennati, M. & Orlando, T. Nitroxide Derivatives for Dynamic Nuclear Polarization in Liquids: The Role of Rotational Diffusion. *The Journal of Physical Chemistry Letters* **11**, 1629, (2020).
- 11 Hu, K. N., Debelouchina, G. T., Smith, A. A. & Griffin, R. G. Quantum mechanical theory of dynamic nuclear polarization in solid dielectrics. *The Journal of Chemical Physics* **134**, 125105, (2011).

- 12 Bajaj, V. S. *et al.* 250 GHz CW gyrotron oscillator for dynamic nuclear polarization in biological solid state NMR. *Journal of Magnetic Resonance* **189**, 251 (2007).
- 13 Vega, S. Fictitious spin 1/2 operator formalism for multiple quantum NMR. *J. Chem. Phys.* **68**, 5518 (1978).
- 14 Ernst, R., R.; Bodenhausen, G.; Wokaun, A. . *Principles of Nuclear Magnetic Resonance in One and Two Dimensions*. 610 (Clarendon Press (Oxford Oxfordshire and New York), 1987).
- 15 Pileio, G. Singlet NMR methodology in two-spin-1/2 systems. *Prog Nucl Magn Reson Spectrosc* **98-99**, 1, (2017).
- 16 Bengs, C. & Levitt, M. H. SpinDynamica: Symbolic and numerical magnetic resonance in a Mathematica environment. *Magn Reson Chem* **56**, 374-414, doi:10.1002/mrc.4642 (2018).
- 17 Redfield, A. in *Advances in Magnetic and Optical Resonance* Vol. 1 1 (Elsevier, 1965).
- 18 Goldman, M. Formal theory of spin--lattice relaxation. *J Magn Reson* **149**, 160, (2001).